Energy Conversion and Management 272 (2022) 116376

Contents lists available at ScienceDirect

Energy Conversion and Management

journal homepage: www.elsevier.com/locate/enconman

Generalized cryptographic image processing approaches using integer-series transformation for solar power optimization under partial shading

Kanasottu Anil Naik [a], Rayappa David Amar Raj [a], Chepuri Venkateswara Rao [a,*], Thanikanti Sudhakar Babu [b]

[a] Department of Electrical Engineering, National Institute of Technology, Warangal 506004, India
[b] Department of Electrical and Electronics Engineering, Chaitanya Bharati Institute of Technology, Hyderabad 500075, India

ARTICLE INFO

Keywords:
Image encryption
Integer sequence
Partial shading
PV array
Reconfiguration

ABSTRACT

Extracting the optimal power from the PV arrays under partial shading conditions (PSC) is challenging. Despite employing bypass diodes, maximum power point trackers, and current injection strategies to mitigate the shading impact, the array yields a considerably sub-optimal output. So, array reconfiguration strategies are employed to overcome this. However, most of the existing static reconfiguration strategies suffer scalability issues, perform arbitrary shade dispersal, and yield distorted array characteristics. Hence, this paper proposes novel PV array configurations based on three distinct image processing strategies employing the integer sequence-based transformation to optimize the array output under PSC. The effectiveness of the proposed strategies is examined using the encryption parameters, histogram analysis and correlation scatter plots. Further, they are implemented for 9 × 9 symmetrical and 5 × 10 unsymmetrical PV arrays and their performance is compared with the 20 existing strategies under 24 distinct shading conditions. Besides, the proposed reconfiguration approaches are validated experimentally for a 4 × 4 PV array in the laboratory and outdoor environments. The qualitative comparison of proposed strategies with state-of-art techniques is discussed in detail. The simulation and hardware results confirm the competency and superiority of the proposed strategies in optimally reconfiguring the PV array yielding the enhancement in output by 32.62%, 20.66%, 16.67%, 14.79%, 13.68%, 13.48% under distinct cases.

1. Introduction

To generate the rated output power, the PV array is connected in various traditional topologies, including Series, Parallel, Series-Parallel, and Total-cross-tied (TCT). Because of its highest power yield under partial shading conditions (PSC) [1] compared to others, the TCT configuration is preferred. The shading of the solar panels is caused by neighboring tall buildings, towers, and passing clouds impacting the array's performance further resulting in the formation of hotspots. To avoid these hotspots, a protection bypass diode is connected in anti-parallel to the PV module. As a consequence, multiple power peaks (MPPs) are created in the array characteristics [2]. The peaks with the highest maximum power are referred to as Global Maximum Power (GMP) points, while the remaining peaks are referred to as local maximum power points. The traditional maximum power point tracking (MPPT) strategies like perturb and observe (P&O), incremental

Abbreviations: ADV, Advanced Sudoku; AI, Artificial Intelligence; CB, Canonical Sudoku; CS, Chaotic Baker; EAR, Electrical Array Reconfiguration; EQT, Equi-digital-Based Transforms; EUT, Euler Zigzag-Based Transform; FP, Futoshiki Puzzle; GMP, Gijswijt's Transformation; GT, Global Maximum Power; HBO, Henon Map; HM, Honey-Badger Optimization; IS, Improved Sudoku; LS, Lo-Shu; MDS, Maximum Power Point Tracking; MPPs, Mean Square Error; MPPT, Multiple Power Peaks; MSE, Multi-Diagonal Sudoku; NA, New Array Scheme; NCI, New Column Index; NOS, Non-Optimized Sudoku; OE, Odd-Even; OEP, Odd-Even-Prime; OS, Optimal Sudoku; OSB, Optimized Sudoku; PSC, Partial Shading Conditions; PSNR, Peak Signal-To-Noise Ratio; P&O, Perturb and Observe; RGB, Red, Green, Blue; SDK, Shift-Modified TCT; SKP, Skyscraper Puzzle; SMT, Spiral Pattern; SPP, Structural Similarity Index; SSI, Sudoku; TCT, Total-Cross-Tied.

* Corresponding author.
E-mail addresses: anilnaik205@nitw.ac.in (K. Anil Naik), dtcdavid2k15@gmail.com (R. David Amar Raj), cvee21209@student.nitw.ac.in (C. Venkateswara Rao), sudhakarbabu@ieee.org (T. Sudhakar Babu).

https://doi.org/10.1016/j.enconman.2022.116376
Received 21 July 2022; Received in revised form 15 October 2022; Accepted 17 October 2022
Available online 28 October 2022

conductance, and other algorithms may not effectively track the GMP as they are easily trapped in the local optimum [3]. To track the GMP under partial shade conditions, a global MPPT technique using improved honey-badger optimization (HBO) for triple-junction PV systems is presented [4]. Under realistic solar radiation, an enhanced P&O MPPT technique for a two-stage grid-interconnected PV system with efficient open-circuit voltage estimate is developed and validated [5]. To track the optimal power peak and improve its resilience and performance, a new triple-stage current-mode MPPT algorithm with fixed and changing current-perturbation phases was developed recently in [6]. These controllers, however, are incapable of harvesting the array's entire capability and can merely track its GMP, regardless of their sophistication. The reconfiguration of PV array is one of the simplest and most practical methods for increasing GMP and reducing power losses [7].

Depending on their operation mode, the array reconfiguration approaches are further categorized into static and dynamic. The dynamic-based techniques are further classified as artificial intelligence (AI)-based, electrical array reconfiguration (EAR)-based, metaheuristic algorithms-based etc. The AI-based dynamic array reconfiguration approaches employing the fuzzy logic [8] and neural network [9] have been experimentally validated to mitigate the mismatch losses under PSC. However, implementing these strategies necessitate numerous switches and sensors and other additional devices for successful operation. For proper functionality, the abovementioned devices are also employed in EAR-based approaches [10–11] and deploying these strategies for considerably larger PV farms is challenging. In order to determine the ideal switching pulse pattern, these approaches generate a vast number of patterns which is a main drawback. In recent days, various population based-metaheuristic algorithms are gaining popularity in designing the switching pattern for reconfiguring the panels. Some of the popular optimization algorithms employed are the genetic algorithm [12], particle swarm optimization [13], butterfly-optimization [14], coyote-optimization [15], moth flame-optimization [16], etc. Despite of their applicability and usefulness in generating the switching pattern, all these metaheuristic algorithms suffer numerous drawbacks and limitations such as large computational stages, time-consuming, convergence issues, multiple parameters, parameter selection challenges, tuning parameters and weighting factor selection challenges, the tendency of being stuck at local optima, huge search space, a large number of iterations, complicated algorithms, randomness involvement, multiple stages to solve, and so on. Notwithstanding their effectiveness, the dynamic reconfiguration procedures necessitate a large number of complex smart devices, switches and sensors, sophisticated methodologies, complex algorithms and regulating units, efficient driving circuits, and systematic monitoring units, all of these add to the system's complexity and expense.

In order to evade all the above-mentioned drawbacks/challenges, the static reconfiguration approaches are adopted. These approaches do not require any additional equipment, complicated methodologies, and complicated algorithms for reconfiguring the array. The static reconfiguration techniques generally include puzzle-based, magic square-based, shift-based, indexing-based, analytical-based, logic-based, chaotic-based, and pattern-based approaches to configure the array. Some of the notable puzzle-based static techniques are based on the sudoku (SDK) [17], optimal sudoku (OS) [18], optimized sudoku (OSB) [19], non-optimized sudoku (NOS) [19], futoshiki puzzle (FP) [20], improved sudoku (IS) [21], skyscraper puzzle (SKP) [22], advanced sudoku (ADV) [23], hyper sudoku [24], canonical sudoku (CS) [25], multi-diagonal sudoku (MDS) [25] puzzle patterns. All these approaches are tested and studied for a 9×9 PV array sizing. The PV panels are configured according to the above-mentioned puzzle patterns to alleviate the row current variation between the rows. However, the major drawbacks of all these techniques are that they cannot be scalable for unsymmetrical PV array sizes. The authors in [26] introduced a magic square reconfiguration approach based on the 3×3 Lo-Shu (LS) grid for mitigating the mismatch losses during PSC. The LS technique, despite yielding a better performance cannot be implemented for the PV array sizes other than $3n \times 3n$. Furthermore, the magic square-based techniques completely fail to be employable for the unsymmetrical arrays. Due to the very narrow application, indiscriminate shade dispersion, and poor scalability, the puzzle-based and magic square-based approaches are not considered to be the best option for reconfiguration.

A one-time fixed shift-modified TCT (SMT) configuration of the PV array is proposed in [27] to dispense the shade to balance the irradiation in distinct rows of an array. Nevertheless, the SMT approach fails to yield consistently superior performance under distinct shading conditions due to its poor arrangement of panels. The authors in [28] proposed an index-based new column index (NCI) strategy to enhance the GMP and improve the array characteristics under shading conditions. However, this technique exhibits highly inconsistent performance under distinct shading conditions. A majority of the aforementioned strategies cannot be scalable to unsymmetrical PV arrays and hence to overcome this major setback, the authors in [29] proposed an analytical-based odd–even (OE) methodology for reconfiguration. The OE approach is applicable to all sizes of PV arrays. An improved version of the OE approach named odd–even-prime (OEP) is proposed in [30] to rectify the shortcoming of the existing OE approach. Both the analytical numbering-based OE and OEP strategies, despite being scalable to all array sizes, exhibit very poor shade dispersion since nearly half of the modules remain in the same rows even after the reconfiguration process. In consequence, the OE and OEP improves the efficiency less than 50 % only. Further, in some of the shading cases, the OE and OEP schemes offer poor performance (due to the high correlation between adjacent panels) even compared to the conventional configurations. The diagonal arrangement of panels through a new array (NA) scheme is proposed in [31] to extract maximum power from the array under PSC. Due to the high correlation between the diagonal panels in an array, this approach fails during the diagonal shading conditions as well as in many other cases.

Very recently, the chaotic mapping-based strategies are gaining the attention of researchers to reconfigure the array effectively. Among them chaotic baker (CB) map strategy is the first proposed strategy to reconfigure the symmetrical PV array [32]. But the CB strategy is also not highly efficient, because even after the reconfiguration nearly 33% of the panels remain in the same rows. Further, it cannot be scalable to the unsymmetrical arrays. To rectify the drawbacks of CB, a novel henon map (HM) strategy is proposed in [33]. The HM technique effectively reconfigures both symmetrical and unsymmetrical arrays, however, it fails under the column shading conditions. In [34], a spiral pattern (SPP) based fixed reconfiguration technique is introduced to maximize the output under shading. Nevertheless, the SPP strategy yield inferior performance under diagonal shading conditions. Moreover, the applicability of SPP for unsymmetrical arrays is not validated. **The following are the major challenges associated with the existing research work:**

- The algorithms used in the dynamic reconfiguration process are complex and involve a weighted-sum methodology, premature convergence issues, complicated searching mechanisms, high computational complexity, optimal weights determination, parameters tuning challenges, and several stages to obtain solutions etc.
- The implementation of these algorithms demands a massive no. of sensors and switches, complex switching matrix, driver circuits, micro-controllers, etc which leads to serious practical and economic feasibility issues.
- Many existing static techniques are predominantly compatible with very few symmetrical sizes of PV arrays and cannot be applicable for asymmetric arrays. However, in practice, most of the established PV arrays are asymmetric. Ascertaining the optimal pattern of the puzzle-based and logic-based strategies from the infinite solution sets is quite tiresome.

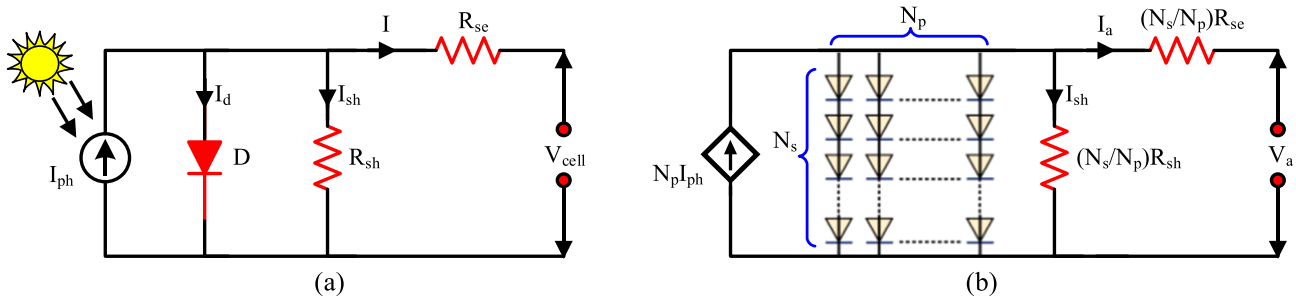

Fig. 1. Equivalent-circuit model of (a) PV cell and (b) PV array.

- The arbitrary shade dispersion obtained through the existing randomized reconfiguration strategies leads to poor/uneven shade dispersal, enhanced mismatch, inconsistent performance, low power enhancement, and underperforms under certain conditions.
- Despite augmenting GMP to a certain extent, the existing strategies exhibit numerous local power peaks in the array characteristics. This imposes a heavy burden on the MPPT controllers while tracking the global maximum power of the array and necessitates sophisticated and costly MPPT controllers.

From the extensive literature review, it is observed that the existing strategies inherit numerous limitations, therefore, this work proposes three novel static reconfiguration topologies to address all the aforementioned drawbacks. **The major highlights of the proposed work are:**

- The proposed approaches disperse the shade intelligently using an integer series-based encryption strategy minimizing the correlation between the adjoining shaded panels in a row/ column and diagonal directions.
- The proposed strategies do not require sensors, switches and other additional equipment for their implementation and successful operation.
- The correlation scatter plot analysis, histogram analysis, and different encryption quality metrics are used to assess and demonstrate the performance of the proposed approaches.
- Most previous methods have been evaluated only with symmetrical PV arrays. The proposed work, however, considers the testing for symmetrical and asymmetrical array sizes, including 9 × 9, 4 × 4, and 5 × 10 PV arrays under 24 various shading conditions.
- The effectiveness of the proposed strategies in comparison to the 20 existing static reconfiguration methodologies has been thoroughly investigated.
- The hardware experimental setup of the proposed configurations has been developed for a 4 × 4 PV array and investigated outdoors and in the indoor laboratory under various artificial shade conditions.

The rest of this article is divided into subsequent sections. The details of the array modeling are covered in Section 2. The proposed methodologies and their application to reconfiguration are elaborated in Sections 3 and 4. The results of various case studies are discussed in Section 5. An exhaustive comparison of various methods is presented in Section 6. The findings derived from the investigation are summarized at the end.

2. Modelling of solar photovoltaic module and array

Numerous PV cells are electrically coupled in series and parallel within a photovoltaic panel. In literature, some PV cell modelling approaches have been introduced, among which the single-diode cell model which is illustrated in Fig. 1(a) is extensively employed due to its easiness [35]. Using current law, the obtained solar PV cell current can be obtained as follows,

$$I = I_{ph} - I_d - I_{sh} \tag{1}$$

here I is cell output current, I_{ph} is light-produced current, I_{sh} and I_d are the currents through shunt resistance and diode. In order to simplify this equation, the total of the saturation current and the shunt leakage current is taken as I_o. The resulting simplified equation is

$$I = I_{ph} - I_o \tag{2}$$

Since photon current is produced when a solar cell absorbs solar radiation, its value is directly correlated with changes in solar irradiance and temperature, and it is given as

$$I_{ph} = (I_{scr} + k_i \Delta T)\frac{G}{G_r} \tag{3}$$

Where k_i is the short-circuit temperature coefficient and I_{scr} is the nominal solar current at nominal climatic condition (25 °C and 1000 W/m^2). G is the nominal solar irradiance under typical ambient circumstances, and G_r is the solar irradiance in W/m^2. ΔT is the variation between the operating temperature (T) and the nominal temperature (T_{ref}). Further, the reverse saturation current of a solar cell [35] will be determined by

$$I_o = I_{rs}\left(\frac{T}{T_{ref}}\right)^3 \exp\left(q\frac{E_{go}}{AK}\right)\left(\frac{\Delta T}{T_{ref}T}\right) \tag{4}$$

where E_{go} is the band-gap energy of the semiconductor material and I_{rs} is the reverse saturation cell current for normal temperature and irradiance levels. Substituting I_{sh} and I_d in Eq. (1), then

$$I_{pv} = I_{ph} - I_0\left[\exp\left(q\frac{V_{pv} + I_{pv}R_{se}}{AKT} - 1\right)\right] - \frac{V_{pv} + I_{pv}R_{se}}{R_{sh}} \tag{5}$$

where I_o is saturation current, q is charge of electron, V_{cell} is cell output voltage, K is Boltzmann's constant, T is operating temperature, A is ideality factor, R_{se}, R_{sh} are series and shunt resistance.

3. Proposed integer sequence-based encryption

The proposed methodology employs the integer sequence-based encryption strategies which are discussed in the subsequent sections.

3.1. Integer sequence

An ordered sequence of integers is termed as an integer sequence in mathematics. It can be defined explicitly by formulating its mth term or by inferentially demonstrating the relationship between its terms. In this paper, three distinct popular integer sequences are employed in the reconfiguration process which are described as follows:

3.1.1. Gijswijt's series

In mathematics, Neil Sloane's Gijswijt sequence [36] is a self-describing mathematical series in which every term enumerates the maximum number of repeated blocks of integers in the series

immediately preceding that particular term. The Gijswijt's series is given as following:

1, 1, 2, 1, 2, 2, 2, 3, 1, 1, 2, 1, 2, 2, 2, 3, 2, 1, 1, 2, 1, 2, 2, 2, 3, 2, 1,……..

The definition of the sequence is identical to that of the Kolakoski sequence, except that rather than counting the longest run of single terms, it enumerates the longest run of the blocks of terms of any length. This sequence is notable for its unusually slower growth rate. Example, the number '4′ first appears in the 220th place, whereas number '5′ first appears near the 1023rd place. By considering the series as a sequence of alphabetical letters of natural numbers, the procedure of generating the terms in the series [37] is described as

$$g(i) = \begin{cases} 1, & if\ i = 1 \\ p, & if\ i = n+1 \end{cases} \tag{6}$$

where p is the greatest natural integer for which the word g(1)g(2)g(3)g(4)….g(n) could be written in the format xy^k for certain words x and y, where y has the non-zero length. The sequence is base-independent. If a sequence of 10 repeating blocks is discovered, the next number in the series will be a single digit '10′, not a '1′ preceded by a '0′.

By definition, the series begins with 1. The length 1 of block of 1′s immediately preceding it in the first place is represented by the '1′ in the second place. The 2 in the 3rd place indicates the length 2 of the 1st and 2nd place's block of 1′s. The series drops for the very first time at this point: The length 1 of block of 2′s in the 3rd place, and also the length 1 of block "1, 2″ spanning the 2nd and 3rd places, are represented by the '1′ in the 4th place. There has been no block of repeated series that is greater than length 1 immediately prior to the 4th place. Since they are disconnected by a different number in the 3rd place, the block of the two 1′s in the 1st and 2nd places cannot be considered for the fourth place. The length 1 of "repeating" blocks such as "1″, "2, 1″, "1, 2, 1″, "1, 1, 2, 1″ that just precedes the 5th place is represented by 1 in the 5th place. Because none of these blocks are replicated, the 5th place is 1. The length of the repeating block of 1′s immediately preceding the 6th place, particularly the ones in the 4th and 5th places, is represented by 2 in the 6th place. The '2′ in 7th place refers to the two repetitions of "1, 1, 2″ block that spans the terms 1 to 3 and thereafter 4 to 6. This "three-number word" appears twice before the 7th place, yielding the 7th place a value of '2′. The length of the repeating block of 2′s immediately prior to the 8th place, notably the 2′s in the 6th and 7th places, is represented by '2′ in 8th place. The number '3′ in the 9th place indicates thrice-repeated blocks of single 2′s just preceding the 9th place, particularly the 2′s in the 6th, 7th, and 8th places.

3.1.2. Euler zigzag series

The Euler Zigzag numbers are a series of integers in which each element is alternately greater or smaller than the one before it [38]. It describes how many alternate permutations are available for n elements. Indicating the total number of alternating permutations on 'n' elements by E (n, k) for which the initial element is k. Then E (1, 1) = 1 and

$$E(n,k) = \begin{cases} 0 & for\ k \geq n\ or\ k < 1 \\ E(n,k-1) + E(n-1,n-k) & otherwise \end{cases} \tag{7}$$

In Eq. (7), E(n,k) represents Entringer number. The number of permutations of (1, 2, 3, 4…, n + 1), beginning with k + 1, which after initially descending, alternately descend and ascend, are known as Entringer numbers [39]. The Entringer numbers, E(n,k) are given by

$$E(0,0) = 1; E(n,0) = 0$$

combined with the recurrence relation E (n, k) = E (n, k-1) + E (n-1, n-k).

The numbers $A(n) = E(n,n)$ are secant and tangent numbers given by the Maclaurin series $\sec(x) + \tan(x) = \tan\left(\frac{\pi}{2} + \frac{x}{2}\right) = A_0 + A_1 x + A_2 \frac{x^2}{2!} + A_3 \frac{x^3}{3!} + A_4 \frac{x^4}{4!} \cdots\cdots = \sum_{n=0}^{\infty} \frac{A_n}{n!} x^n$ where A_n represents Euler zigzag numbers [38]. The Euler zigzag number sequence is followed as 1, 1, 1, 2, 5, 16, 61, 272, 1385, 7936, 50521, 353792……..

For all even numbers of 'n',

$$A_n = (-1)^{\frac{n}{2}} E_n,$$

Where E_n denotes the Euler number; and ∀ odd numbers of 'n',

$$A_n = (-1)^{\frac{n-1}{2}} \frac{2^{n+1}(2^{n+1}-1)B_{n+1}}{n+1},$$

Where B_n denotes a Bernoulli number.

3.1.3. Equidigital number series

A natural number containing the same number of digits as that of the number of digits in its factorisation in the selected number base, which would include exponents however excluding exponents equal to one, is called an equidigital number in number theory [36,40]. In base 10, equidigital numbers comprise 1, 2, 3, 5, 7, and 10. Further, all prime numbers seem to be equidigital numbers in any base.

Let $K_b(n) = \lfloor \log_b n \rfloor + 1$, and b > 1 where, 'b' is a number base, $K_b(n)$ is the number of digits in a natural number 'n' for b. The integer - factorization of a natural number 'n' is

$$n = \prod_{\substack{p|n \\ p\ prime}} p^{v_p(n)}$$

$$K_b(n) = \sum_{\substack{p|n \\ p\ prime}} K_b(p) + \sum_{\substack{p^2|n \\ p\ prime}} K_b\left(v_p(n)\right)$$

where $v_p(n)$ represents p-acidic order of integer of 'n' [39]. The first few equidigital numbers are 1, 2, 3, 5, 7, 10, 11, 13, 14, 15, 16, 17, 19, 21, 23, 25, 27, 29, 31, 32, 35, 37, 41…. The aforementioned three integer sequences are used in the transformation matrix of the encryption strategies which are detailed in the subsequent sections.

3.2. Cryptographic image encryption

In cryptography, image encryption is the process of effectively rearranging the pixels to obscure the image's visual content and disrupt the correlation between the adjacent pixels [41]. The pixel values often remain the same while being rearranged. Several image encryption techniques have recently been proposed. Confusion and diffusion are the two phases that the majority of image encryption techniques adopt. The pixel coordinates are permuted using a scrambling approach in the confusion phase, and the pixel values are altered using an inverse function in the diffusion phase. An efficient encrypting algorithm reduces this correlation, which is substantially correlated between adjacent pixels in an image, to almost zero. The integer sequence transformation such as Luca's transform, Fibonacci transform etc. may also be used to perform the matrix-based scrambling [42].

3.3. Encryption based on generalized transformation matrix

The fundamental transformation is represented by Eq. (8)

$$\overline{A}_K = Q\overline{A}_{K-1} mod\ \overline{M}, k \in Z^+ \tag{8}$$

In the above equation (8), 'Q' is the scrambling transformation matrix of dimension m × n whose elements are all positive integers, $\overline{A}_K$, $\overline{A}_{K-1}, \overline{M}$ are m × 1 vectors and $0 < a_{i,j} \leq M_{j-}$ for $i = k-1, k$ and j = 1,2,3, ….,n considering $\overline{A}_{K-1} = (A_{k-1,1}A_{k-1,2}A_{k-1,3}\cdots..A_{k-1,n})$ and $\overline{A}_K = (A_{k,1}A_{k,2}A_{k,3}\cdots\cdots..A_{k,n})^{'}$, $\overline{M} = (M_1M_2M_3\cdots\cdots..M_n)^{'}$ represents module vector where M_j are non-negative integers denoting the maximum limit of the respective a_{ij}=(i, j = 1,2,3…..). The number of scrambling times of a digital image is represented by a non-negative integer k. Further, the symbol '+' signifies the set of non-negative integers. The Eq. (8) can be transformed into Eq. (9) in the case of an equal module, which is known

as an equi-modulo transformation, i.e, $\overline{M} = (N\ N\ N \cdots N)^{'}$.

$$\overline{A}_K = Q\overline{A}_{K-1} mod\ M, k \in Z^+ \tag{9}$$

3.4. Transformation matrix-based two-dimensional mapping using integer series

One of the easiest methods for encrypting the image with dimensions (P × Q), where P denotes the image's height and Q its breadth, is two-dimensional mapping. In the digital image encryption process, the pixel coordinates of an image are rearranged by using a transformation matrix [43]. The transformation matrix stretches and shears the original image realigning its pixels for encryption. Eq. (10) describes the form of an invertible mapping that is used in matrix-based encryption.

$$\begin{pmatrix} x(i+1) \\ y(i+1) \end{pmatrix} = \begin{pmatrix} b_{00} & b_{01} \\ b_{10} & b_{11} \end{pmatrix} \times \begin{pmatrix} x(i) \\ y(i) \end{pmatrix} mod\ M \tag{10}$$

where x(i) and y(i) ∈ [0, M−1) × [0, M−1). The Eq. (10) encrypts the image if $(b_{00} \times b_{11}) + (b_{01} \times b_{10}) = \pm 1$ making the scrambling invertible. x(i), y(i) and x(i + 1), y(i + 1) are the original and relocated pixel coordinates of the image, M is the order of the image. The three integer sequences discussed in Section. 3.1 have the distinctive property of uniformity. It is remarked that the 2 × 2 matrix constituted up of the first four succeeding terms of the Gijswijt's, Equidigital, and Euler zigzag number series is a unimodular matrix and further include many of such sets, which in effect repositions the pixel coordinates of matrix and can therefore be utilized for encrypting the image. Employing these approaches improves the effectiveness of encryption by dispersing all nearby pixels such that they are uniformly spaced from one another. The basic structure of two-dimensional mapping-based encryption is given in Algorithm. 1.

Algorithm 1. Basic Structure of 2D Mapping-based Encryption

```
Input:      Original image I (i, j) whose dimension is (P × Q)
Generate coordinates × (i, j) and y (i, j) of the image
  for       each pixel I (i, j) do
            I' (x (i, j), y (i, j)) = I (i, j)
  end for
Output:     Encrypted image I' (i, j)
```

The cryptographic image encryption process typically uses a transformation matrix to transform the pixel locations [43]. The transformation matrices obtained by employing the integer sequences successfully relocate the pixels. The integer series inspired Gijswijt's sequence-based transform improves encryption by dispersing all nearby pixels such that they are equally spaced from one another maintaining uniformity. As mentioned earlier, the transformation matrix formed by the four subsequent terms of the Gijswijt's sequence is indeed a unimodular matrix facilitating effective repositioning of the matrix's pixel coordinates and thus utilized for image encryption. The mapping $G : T^2 \rightarrow T^2$ that represents the generalized Gijswijt's transform (GT) is as follows:

$$\begin{bmatrix} x(i+1) \\ y(i+1) \end{bmatrix} = \begin{bmatrix} G_i & G_{i+1} \\ G_{i+2} & G_{i+3} \end{bmatrix} \begin{bmatrix} x(i) \\ y(i) \end{bmatrix} \text{mod M} \tag{11}$$

where × and y ∈ {0, 1, 2, 3,….N-1}, $x(i), y(i)$ are the old pixel coordinates and $x(i+1), y(i+1)$ are the new pixel coordinates of the image, G_i is i^{th} term in a Gijswijt's series, 'mod' is the arithmetic modulo operator and M represents the size of the image in Eq.(11). Employing the Gijswijt's transformation matrix in encryption process, the old pixel locations are replaced by the new locations. By representing $\begin{bmatrix} G_i & G_{i+1} \\ G_{i+2} & G_{i+3} \end{bmatrix}$ as GT_i, the first, second and third transformation matrices formed by the consecutive terms of the Gijswijt's series are given as

$$GT_1 = \begin{bmatrix} G_1 & G_2 \\ G_3 & G_4 \end{bmatrix} = \begin{bmatrix} 0 & 1 \\ 1 & 1 \end{bmatrix}; GT_2 = \begin{bmatrix} G_2 & G_3 \\ G_4 & G_5 \end{bmatrix} = \begin{bmatrix} 1 & 1 \\ 1 & 2 \end{bmatrix}; GT_3 = \begin{bmatrix} G_3 & G_4 \\ G_5 & G_6 \end{bmatrix} = \begin{bmatrix} 1 & 1 \\ 2 & 2 \end{bmatrix}; \cdots$$

For various values of 'i', there exist many sets of the transformation matrices of the Gijswijt's series. The encryption process can be additionally improved by iterating Eq. (11) employing the operation given in Eq. (12)

$$\begin{bmatrix} x(i+1) \\ y(i+1) \end{bmatrix} = \begin{bmatrix} G_i & G_{i+1} \\ G_{i+2} & G_{i+3} \end{bmatrix}^n \begin{bmatrix} x(i) \\ y(i) \end{bmatrix} \text{mod M}, n \geq 2 \tag{12}$$

Algorithm 2: Gijswijt's/ Euler/ Equidigital Transform-Based Encryption

```
Procedure 2D mapping based cryptographic encryption
Input: Matrix of dimension (rows, columns)
Output: Optimal encrypted matrix with least correlation
Determine no. of rows, columns, size of matrix
Find out total number of shifts in matrix
Determine minimum number of rows and columns
Initialize the pixel coordinates (X, Y)
while (termination criteria is not met) do
//Implementation of Gijswijt's/ Euler/ Equidigital transform-based encryption
Extract largest symmetrical sub-matrix from (X, Y) coordinates
For x = X to (X + min [rows, columns]) do
    for y = Y to (Y + min [rows, columns]) do
        obtain new coordinates of 'x' from Eq. (12/13/14)
        obtain new coordinates of 'y' from Eq. (12/13/14)
        Swap old pixel coordinates with new pixel coordinates (x, y)
    end for
end for
```

(continued on next page)

(a) (b)

Fig. 2. (a) Original image of living room and (b) its respective encrypted image.

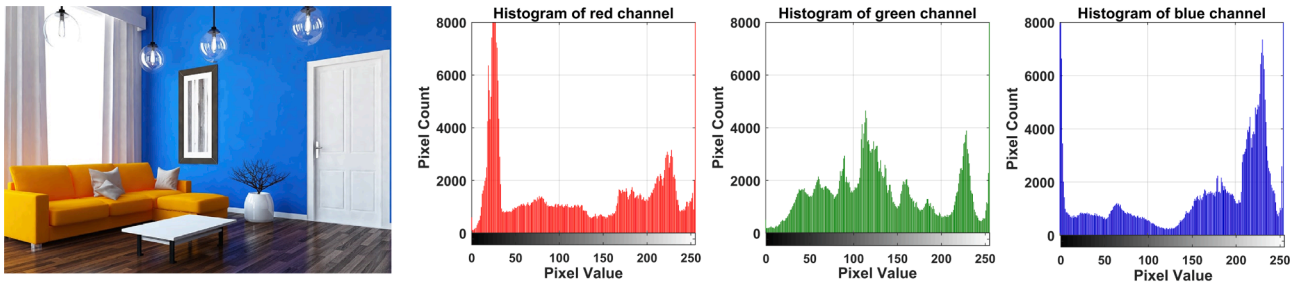

Original living room image and its corresponding histogram of RGB channels

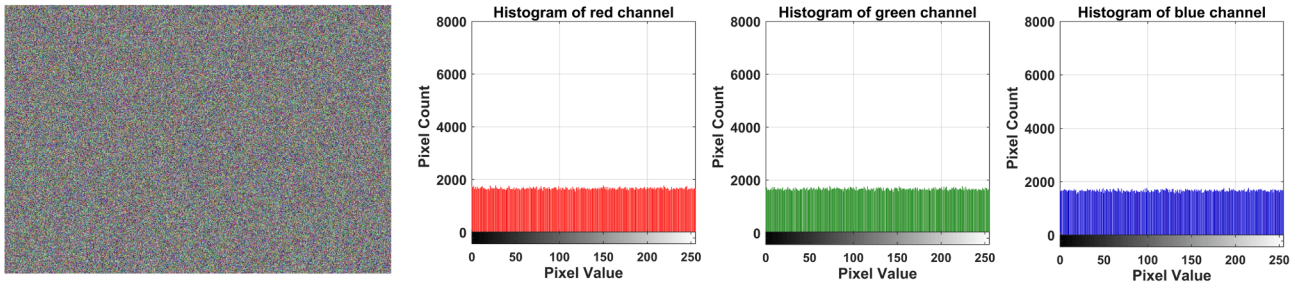

Encrypted image and its corresponding histogram of RGB channels

Fig. 3. Histogram analysis of original and encrypted images.

(*continued*)

```
for i = 1 to maximum shifts do
        Apply Gijswijt's/ Euler/ Equidigital transform-based encryption
        if number of rows < number of columns then
        Apply row coordinate shifting by one
        Else
        Apply column coordinate shifting by one
end for
end while
end procedure
```

By using Eq. (12), the pixels are effectively rearranged mitigating the correlation between them resulting in successful encryption. Likewise, the similar integer sequences such as Euler zigzag and equidigital numbers can also form the unimodular transformation matrices thereby suitable to be employed for encryption. The two-dimensional mapping of the Euler zigzag-based transform (EUT) and equidigital-based transforms (EQT) can be similarly obtained as follows

$$\begin{bmatrix} x(i+1) \\ y(i+1) \end{bmatrix} = \begin{bmatrix} EU_{\mathrm{i}} & EU_{\mathrm{i+1}} \\ EU_{\mathrm{i+2}} & EU_{\mathrm{i+3}} \end{bmatrix}^{n} \begin{bmatrix} x(i) \\ y(i) \end{bmatrix} \bmod \mathrm{M}, \mathrm{n} \geq 2 \tag{13}$$

Where EU_i is i^{th} term in a Euler zigzag series,

$$\begin{bmatrix} x(i+1) \\ y(i+1) \end{bmatrix} = \begin{bmatrix} EQ_{\mathrm{i}} & EQ_{\mathrm{i+1}} \\ EQ_{\mathrm{i+2}} & EQ_{\mathrm{i+3}} \end{bmatrix}^{n} \begin{bmatrix} x(i) \\ y(i) \end{bmatrix} \bmod \mathrm{M}, \mathrm{n} \geq 2 \tag{14}$$

Where EQ_i is i^{th} term in a Equidigital number series. Improper selection of elements in designing the transformation matrix (violating the principles of the unimodular matrix) formed by the consecutive integers of the proposed sequences leads to misleading/sub-optimal output. Hence, the selection of the transformation matrix formed must be selected appropriately for optimal output. The generalized pseudocode of the Gijswijt's/ Euler/ Equidigital transform-based encryption algorithms is given in Algorithm. 2. The aforementioned proposed strategy based on two-dimensional mapping has been implemented on the image of a living room and the obtained encrypted image is shown in Fig. 2. It is noted from the figure that the adjacent pixels of the original image are uniformly scattered mitigating the correlation between them (in horizontal, vertical, and diagonal directions) leading to a secure image encryption. The horizontal, vertical, and diagonal correlation plots of the original image are presented in Fig. 5 (a), and the correlation plots of the encrypted image are further shown in Fig. 5(b).

4. Performance evaluation of proposed encryption strategies

To assess the encryption performance of scrambling algorithms, correlation coefficient, histogram analysis and computational time are often used tools which are discussed as follows:

4.1. Histogram analysis

The histogram is a graph or a plot which gives the idea about the intensity distribution of an image. In order to assess how well the proposed encryption strategy performs at preventing an intruder from attempting to access the characteristic pixels of the image, histogram analysis is a crucial security-based analytical tool [43] in image encryption approaches. The histogram of Red Green Blue (RGB) channels of original image and encrypted image is shown in Fig. 3, and it is remarked that the encryption algorithm generates flat/uniform histograms, yielding uniform intensity distribution implying that it has strong resistance to various statistical attacks.

4.2. Correlation analysis

The digital images' 8-bit nature constitutes a strong correlation between the neighboring pixels in all directions. This correlation can be highly mitigated by effective pixel dislocation in image encryption schemes. In the present study, the image is scrambled using the three distinct integer sequence-based transforms, and the performance of these encryption approaches is evaluated using the correlation coefficient [43]. An encrypted image obtained by a successful encryption approach should have zero correlation ideally. The correlation coefficient of the pixels in an encrypted image can be obtained as follows

$$r(A,B) = \frac{cov(A,B)}{\sigma(A)\sigma(B)},$$

where cov(A, B) is covariance of A and B, σ() represents standard deviation, A and B are two neighboring pixel sequences. Further, r(A, B) is horizontal, vertical coefficient, and diagonal correlation coefficients, respectively, when B is each A's neighboring horizontal, vertical, and

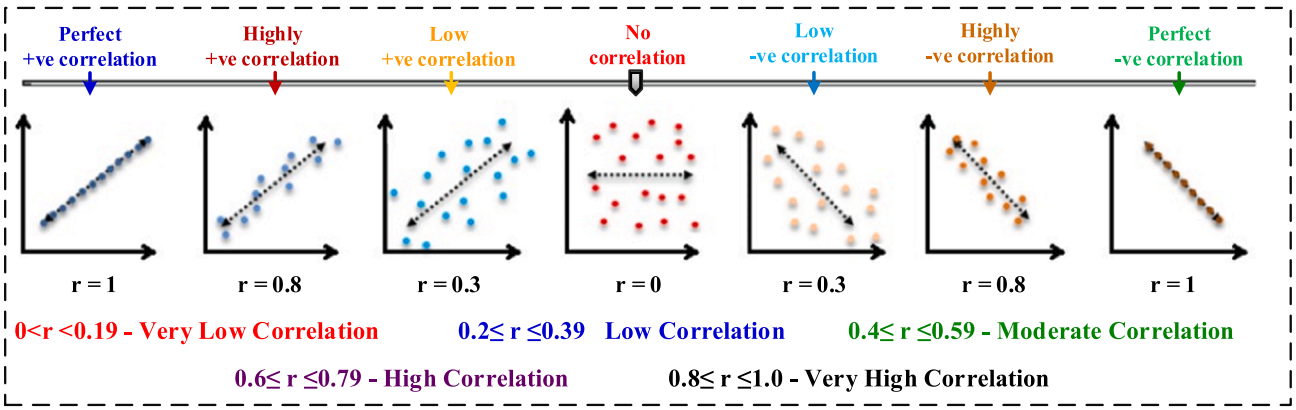

Fig. 4. Range of correlation coefficient (r).

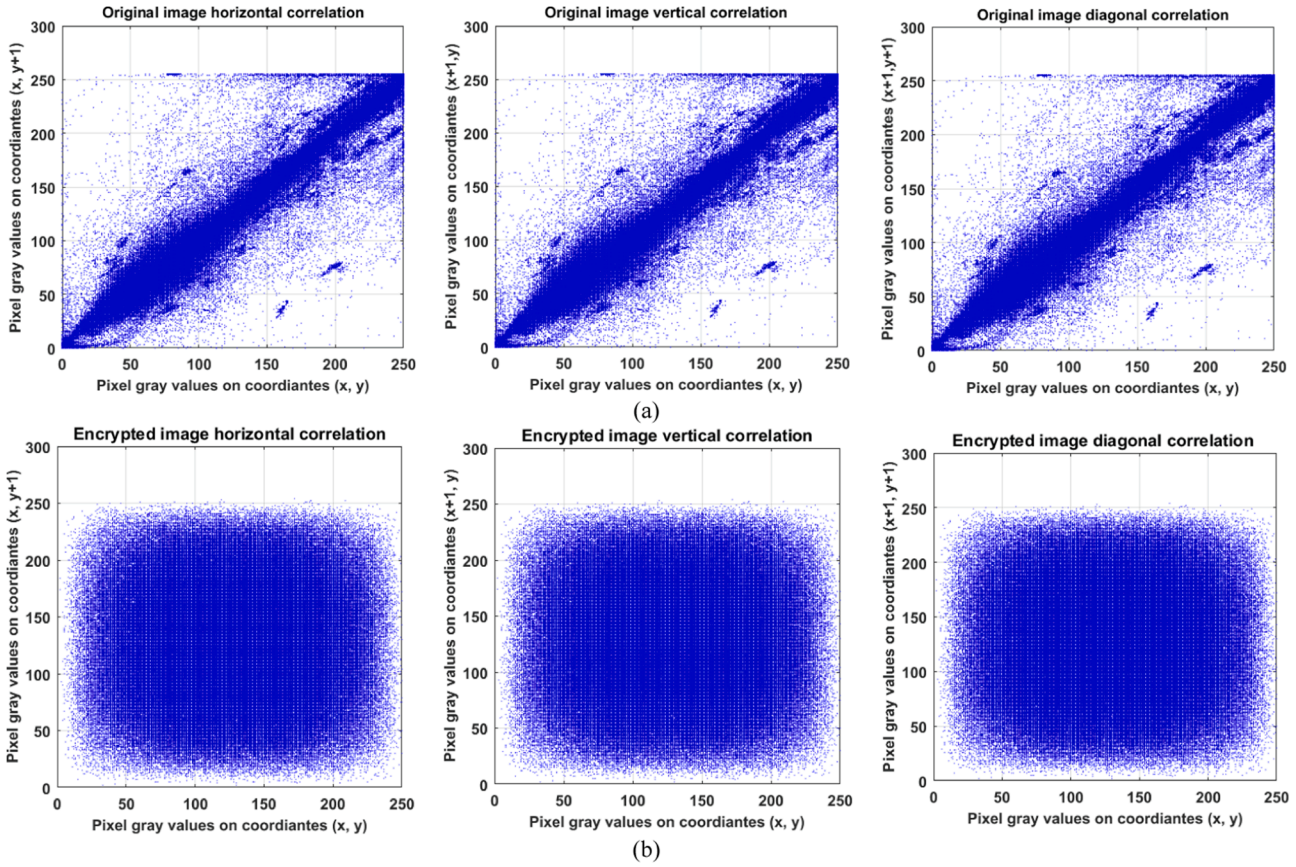

Fig. 5. Correlation scatter plots in horizontal, vertical, and diagonal directions of (a) original and (b) encrypted image.

diagonal pixel.

The correlation between two neighboring pixels is then determined using the r(A, B) function in terms of the horizontal, vertical, and diagonal directions. There is a strong correlation between the neighboring pixels if r(X, Y) is closer to one. In contrast, the correlation between the neighboring pixels is low if r(X, Y) is close to zero. Generally, the original image's correlation coefficient is almost one, which means that the correlation between different orientations in the image is very high. The range of correlation coefficient is shown in Fig. 4. The pixels of an image are distributed uniformly in the encrypted images in horizontal, vertical, and diagonal directions. The distribution of pixels represented by correlation scatter plots before and after encryption of the living room image is shown in Fig. 5 taking the old coordinates on x-axis and new coordinates on the y-axis. The original 9×9, 5×10, and 4×4 matrices and the obtained encrypted matrices by the proposed GT, EUT, and EQT approaches are shown in Fig. 6. As noted in Table. 1, the encrypted image's correlation coefficients, however, are nearly zero in all directions, which suggests that there is hardly any correlation between the adjacent pixels signifying that the encryption effect produced by the proposed encryption strategies is effective and resistant to statistical attacks. The optimal values (from Table.1) of various metrics [44] such as mean square error (MSE), peak signal-to-noise ratio (PSNR), correlation, structural similarity index (SSI) obtained by the proposed approaches proves them to be efficient to be employed for intelligent reconfiguration.

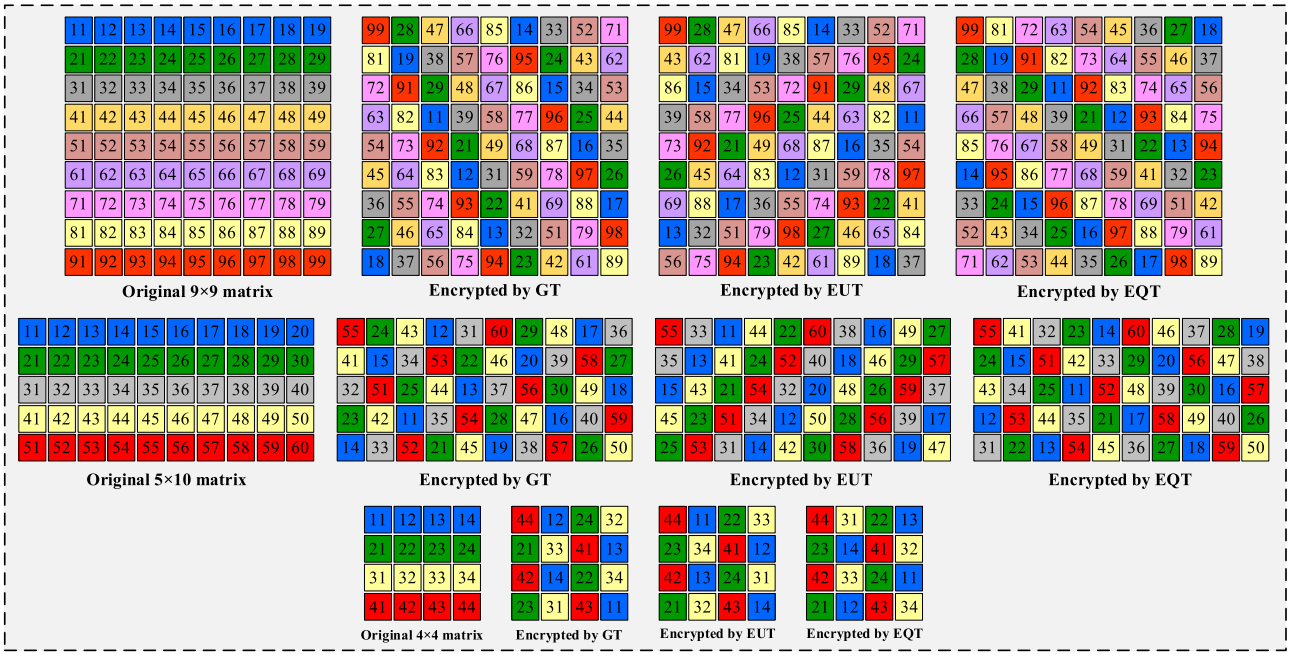

Fig. 6. Original matrices and the proposed GT, EUT and EQT approaches-based encrypted matrices.

Table 1
Distinct encryption performance metrics of proposed techniques for different array sizes.

Array	Technique	Correlation	MSE	SSI	PSNR
9 × 9	GT	+ 0.00001	1346.7	+0.02621	−31.2926
	EUT	−0.000990	1378.1	−0.00570	−31.2969
	EQT	+ 0.00001	1346.7	+0.02810	−31.2926
5 × 10	GT	+0.03000	404.00	−0.00481	−26.0638
	EUT	+0.02521	406.10	+0.00022	−26.0853
	EQT	+0.03000	404.30	+0.00774	−26.0638
4 × 4	GT	−0.01980	257.500	−0.01947	−24.1078
	EUT	−0.01980	257.500	−0.01947	−24.1078
	EQT	−0.01980	257.500	−0.01947	−24.1078

4.3. Distinctiveness and application of integer-based encryption strategies in reconfiguration

Encrypting the digital image for better security decorrelates the adjacent pixels by adding confusion and diffusion to it as the image constitutes a lot of pixels grouped together having a strong correlation between them. Likewise, the PV array also constitutes a number of PV panels connected in series and parallel. When a particular row or portion of the array is shaded, there exists a considerable mismatch with respect to the unshaded row/ portion of the array. Dispersing the shade over distinct rows and reducing its effect in a particular row is the efficient solution to enhance the GMP. The distinctive characteristic feature of decorrelating the adjoining pixels of an image in encryption is the best possible solution for reconfiguring the array to reduce the correlation between the neighboring shaded panels in a row thereby reducing the mismatch between irradiation of distinct rows of a PV array. For implementing this unique feature of encryption, an individual PV panel is considered as a pixel and the total PV array as the image consisting of many pixels. The encryption-based reconfiguration is executed by configuring the panels of an array according to the arrangement of the encrypted matrix obtained by the proposed Gijswijt's/ Euler/ Equi-digital transform-based algorithms.

Unlike most existing reconfiguration strategies that disperse the shade randomly, employing the encryption-based algorithms perform intelligent shade dispersal for equalizing the irradiations. This guarantees consistent and superior performance under any type of shading condition contrasting the existing strategies. The electric circuital interconnections remain the same while the solar PV array is reconfigured according to a predefined rearranged matrix pattern evolved using the proposed transform-based algorithms. By executing this, the shading

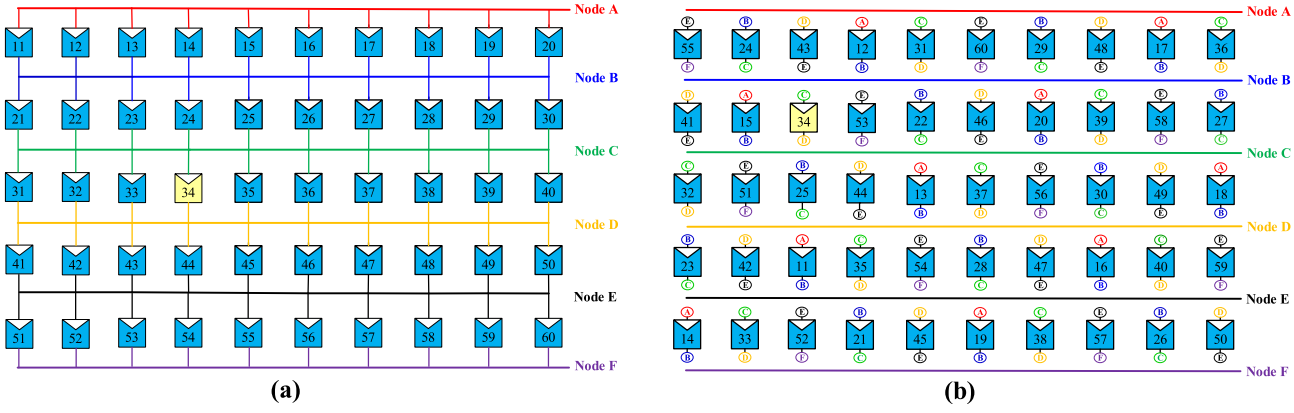

Fig. 7. Topology arrangement of (a) conventional TCT and (b) proposed GT-based array configurations.

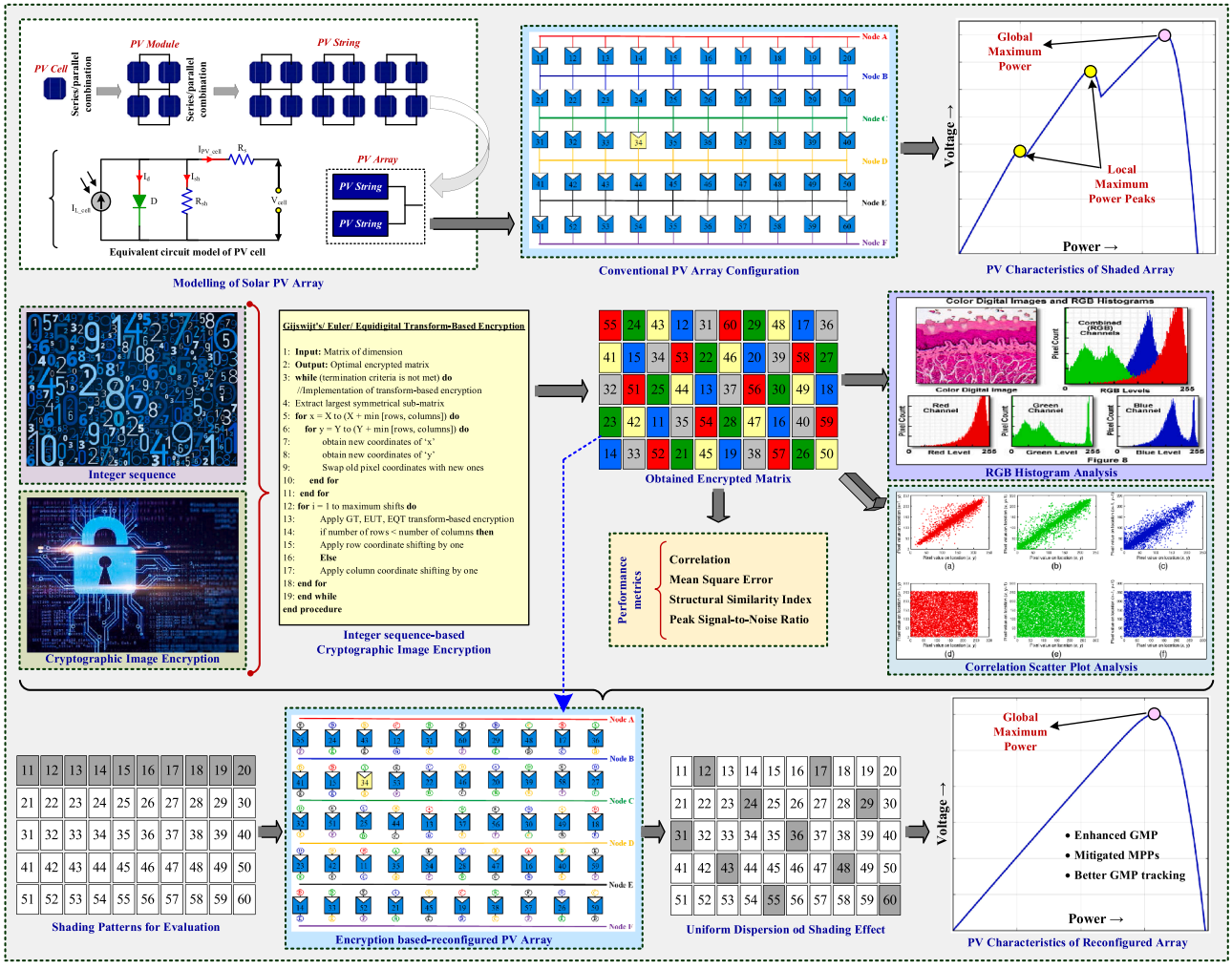

Fig. 8. General overview of the proposed encryption-based reconfiguration strategy.

effect is mitigated highly while the array's electrical properties are preserved. The architectural topological structure difference between TCT and proposed GT-based configurations is demonstrated in Fig. 7, where the panels of the TCT-configured array are rewired electrically or repositioned physically based on the proposed rearranged matrices.

In the TCT-configured PV array, as shown in Fig. 7(a), panel number "34″ is in the third row and fourth column (between Node-C and Node-D). However, based on the obtained rearranged matrices, this panel is now positioned in the second row and third column, or between Node-B and Node-C, as shown in Fig. 7(b). Likewise, all of the PV panels are effectively/optimally configured to distribute the shadow uniformly using the encrypted matrices. For example, if the PV panels (PV55, PV24, PV43, PV12 and PV31) of the first row of the reconfigured array are shaded, this row-wise shade is disseminated to all rows, balancing the irradiation across the rows and mitigating the mismatch as these panels are physically positioned in the first row while are electrically interconnected to different rows. The general overview of the proposed encryption-based reconfiguration strategy is shown in Fig. 8.

5. Results and discussion

The efficacy of the proposed GT, EUT, and EQT approaches has been experimented with and analyzed in MATLAB for distinct TCT-configured symmetrical 9 × 9, 4 × 4, and unsymmetrical 5 × 10 PV array sizes and their effectiveness is compared with the 20 existing strategies under 24 distinct shading conditions. A KG200GT-200 W PV panel has been used

Table 2
Obtained GMP (in Watt) for 9 × 9 array under Case-1 to Case-5.

Approach	Case-1	Case-2	Case-3	Case-4	Case-5
TCT [8]	12,441	12,441	11,769	10,173	13,704
SDK [17]	13,491	13,403	10,943	13,387	12,903
OS [18]	13,490	13,648	11,635	13,678	13,234
OSB [19]	13,681	13,385	12,239	13,493	12,781
NOS [19]	13,491	13,259	11,431	13,464	13,403
FP [20]	13,491	13,679	10,748	13,387	13,302
IS [21]	13,681	13,487	11,922	13,366	12,191
SKP [22]	13,491	13,491	11,635	13,491	12,937
ADV [23]	13,491	13,387	11,943	13,335	13,488
CS [25]	13,481	13,403	10,947	13,404	12,796
MDS [25]	13,491	12,924	11,943	13,491	12,936
LS [26]	13,491	13,403	11,649	13,491	11,649
SMT [27]	13,260	13,258	11,413	13,471	12,796
NCI [28]	13,381	13,319	10,373	12,760	12,652
OE [29]	12,911	12,171	8968.7	12,139	12,733
OEP [30]	12,190	12,180	11,633	13,319	12,890
NA [31]	12,884	12,884	9684.4	12,884	10,663
CB [32]	13,262	13,262	11,413	13,262	13,704
HM [33]	13,295	13,295	11,770	12,884	13,704
SPP [34]	12,884	12,884	9611.1	13,522	12,171
Proposed GT	13,694	13,694	12,239	13,491	13,704
Proposed EUT	13,694	13,694	12,240	13,491	13,704
Proposed EQT	13,694	13,694	12,240	13,491	13,704

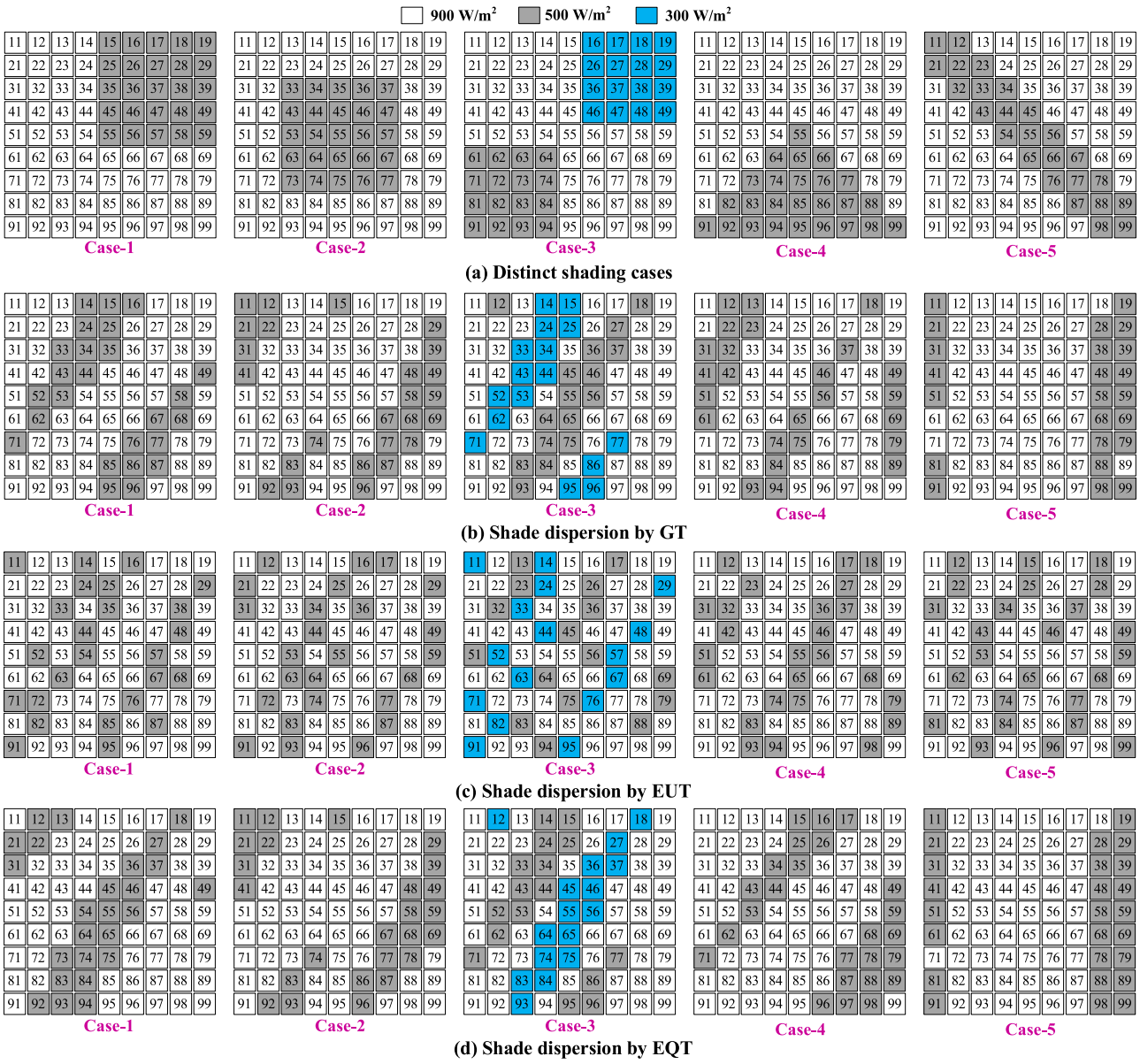

Fig. 9. (a) Different shading cases and respective shade dispersal by (b) GT, (c) EUT, (d) EQT for 9 × 9 array.

throughout the analysis. The respective shaded and unshaded PV panels are considered to obtain the solar irradiance of (500 W/m^2, 300 W/m^2) and 900 W/m^2 in the simulation studies.

- The obtained results of the proposed approaches for a 9 × 9 array are compared with the conventional TCT[8], and existing SDK[17], OS [18], OSB[19], NOS[19], FP[20], IS[21], SKP[22], ADV[23], CS [25], MDS[25], LS[26], SMT[27], NCI[28], OE[29], OEP[30], NA [31], CB[32], HM[33], SPP[34] techniques under Case-1 to Case-5 shading scenarios.
- The effectiveness of the proposed approaches is further verified for the 5 × 10 unsymmetrical PV array under Case-11 to Case-16 and their performance is compared with the TCT [8], OE [29], OEP [30] configurations.

The obtained GMP values of various configurations of a 9 × 9 symmetrical PV array during the considered shading cases are presented in Table.2. The inclusive quantitative and qualitative comprehensive analysis of the proposed configurations is detailed in the subsequent sections:

5.1. Study on symmetrical 9 × 9 PV array

During shading Case-1, the top-right part of the array is considered to be shaded where the shaded and unshaded panels receive the irradiation of 500 W/m^2 and 900 W/m^2. It is remarked from Fig. 9 that the proposed GT, EUT, and EQT approaches exhibit uniform shade dispersion over the array thereby alleviating the mismatch between distinct rows. The PV characteristics of all the studied configurations are shown in Fig. 10. The TCT configuration yields the GMP of 12441 W, whereas the proposed approaches yield 13694 W which is the highest among all the existing ones. The GMP is enhanced by 10.07% employing the proposed techniques. Followed by the proposed ones, the existing OSB and IS exhibit 9.97% gain. However, both OSB and IS are not scalable to unsymmetrical arrays. Whereas the existing puzzle-based SDK, NOS, FP, OS, SKP, LS, ADV, CS, and MDS exhibit an enhancement of nearly 8.3%. Again, these techniques are also not scalable for all array sizes. The recently proposed chaotic CB and HM strategies offer the enhancement in the range of (6.5–6.6)%. Further, the OE technique despite being scalable to all arrays yields only 3.78% gain due to its poor and indiscriminate shade dispersion. The OEP strategy, which is the improved version of

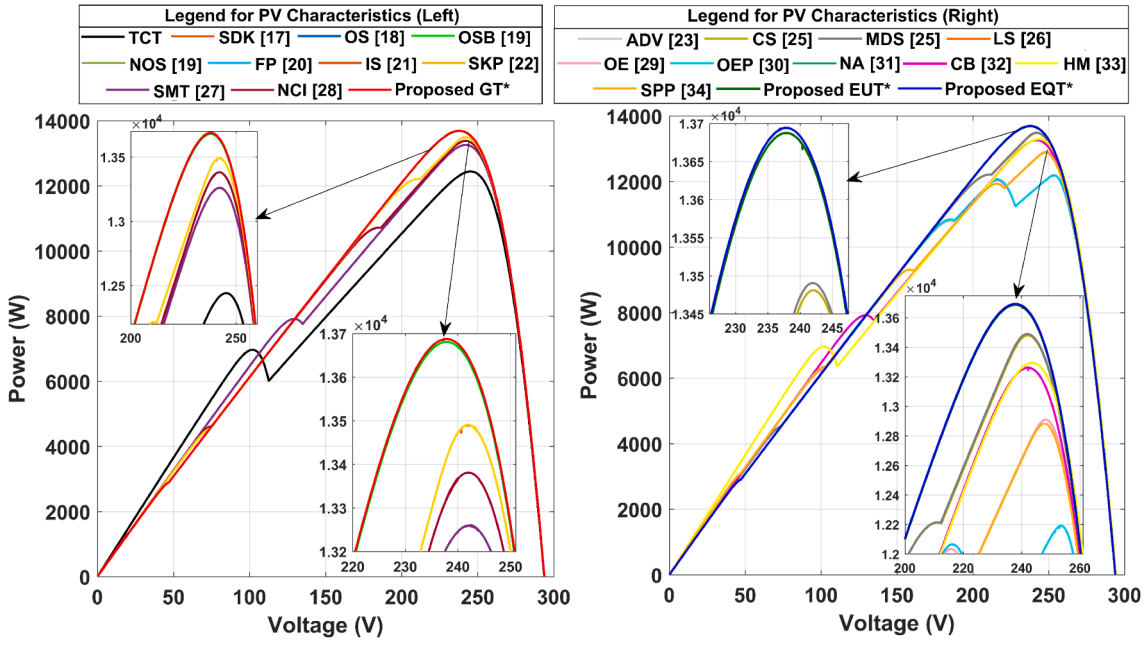

(a) Case-1

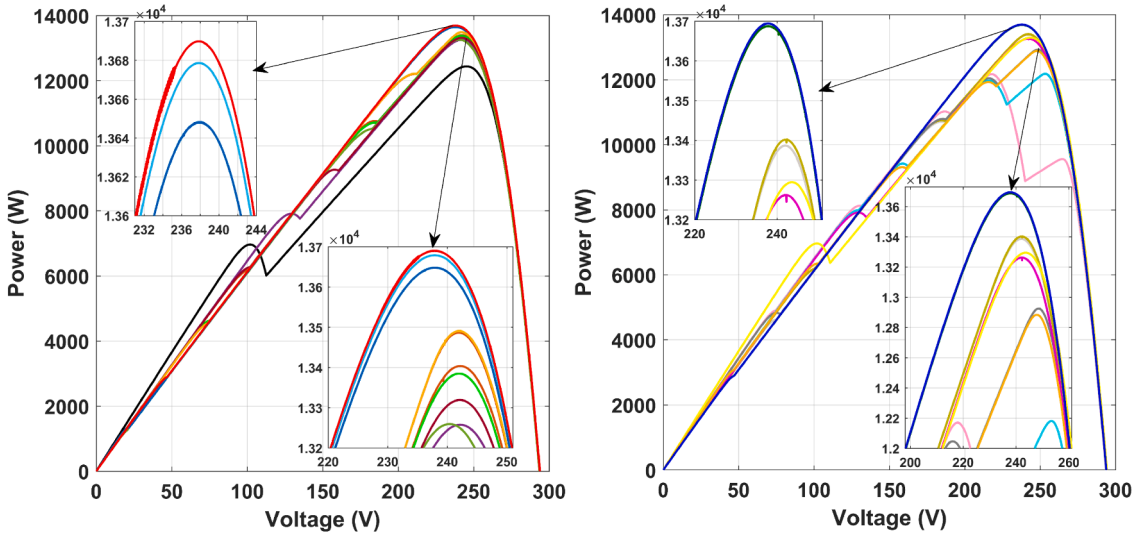

(b) Case-2

Fig. 10. Power-voltage (PV) characteristics of 9 × 9 symmetrical array under (a) Case-1 to (e) Case-5.

OE, fails significantly under Case-1 lowering the GMP by 2.02%. On contrary, the proposed techniques yield the highest GMP with the improved array characteristics as shown in Fig. 10.

The shading pattern considered in Case-2 is the same as in Case-1, but it occurs at a different location in the array, as illustrated in Fig. 9. Even in this case, the proposed approaches yield the highest GMP of all, with a 10.07% increase in GMP. The performance of all other techniques, on the other hand, has been varied, exhibiting different values of enhancement. On contrary, the performance of the proposed configurations is unaffected by the change in the shadow location in the array. The existing OSB and IS, which generated a 9.97% gain in Case-1, now yield 7.59 and 8.41 % gains, respectively. The existing OS and FP techniques yield about 9.7% gain. However, both of these techniques are not implementable for all array sizes. The performance of the puzzle-based IS and SKP techniques are on par with each other exhibiting about 8.41% gain. The recently reported MDS enhances the GMP by 8.44% in Case-1, but in Case-2 it enhances by only 3.88% exhibiting highly inconsistent performance. Further, the NA and SPP strategies yield very little enhancement of only 3.56%. Both the number-based OE and OEP approaches exhibit quite unsatisfactory performance reducing the GMP by 2.17%. The arbitrary reconfiguration process of existing approaches is primarily responsible for this inconsistency and variable performance.

In the Case-3 shading pattern, the shaded panels of the array are considered to be shaded by two irradiation levels. Under this case, very few reconfiguration techniques exhibit GMP enhancement among which the proposed GT, EUT, and EQT, and the existing OSB strategies take first place enhancing the GMP by 4.01%. Notwithstanding, the existing OSB has very limited application as mentioned in Section.1. Besides, the recently developed IS, ADV, and MDS strategies yield only about a 1.3% increase. Very recently reported chaotic-based-HM failed in augmenting the GMP and its performance is on par with the conventional TCT.

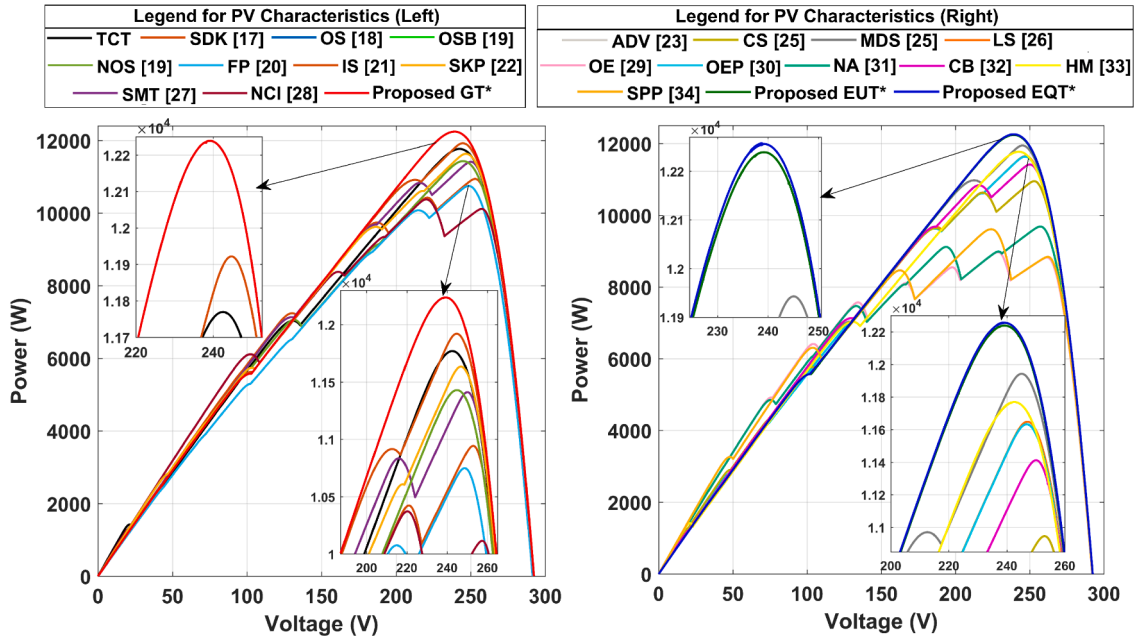

(c) Case-3

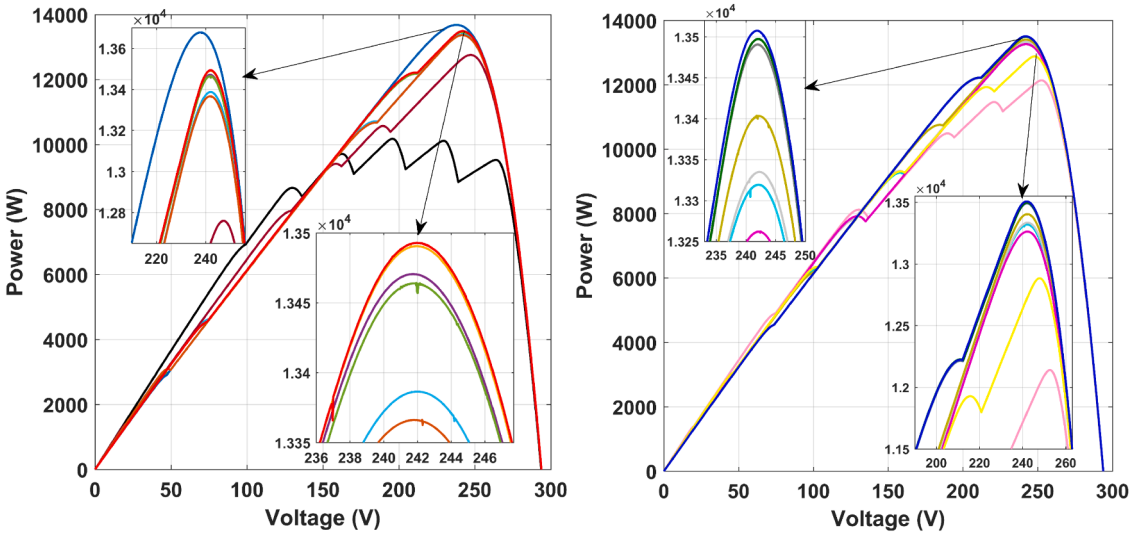

(d) Case-4

Fig. 10. (*continued*).

Further, the puzzle-based OS, SKP, and LS techniques show inferior performance lowering the output by 1.14%. The existing SMT, NOS, and CB configurations generate about 3.02 % less GMP than that of the benchmark TCT configuration. Furthermore, the existing logic-based CS and FP offer the most undesirable performance decreasing the output by 8.68% and 6.89% respectively. Similarly, due to the uneven shade dispersion by SPP, NA, and NCI approaches, they lower the output drastically by 18.34%, 17.71%, and 11.86% respectively. Despite being adaptable to all PV array sizes, the analytical-based OE delivers the most unsatisfactory results among all, diminishing the GMP by 23.79 %. Even under varying irradiation levels at distinct locations of PV array (from Cases-2,3), the proposed techniques proved their effectiveness in delivering consistent behaviour.

The lower part of the array is considered to be shaded in a triangular pattern as shown in Case-4. During this case, the proposed approaches including most of the existing ones-perform well in distributing the shade to mitigate the shading losses and mismatch in row currents by balancing the irradiation. The existing OS strategy despite yielding the highest GMP by delivering 34.45% enhancement fails to be employable for asymmetric PV arrays. On par with, the proposed approaches enhance the output by 32.63% mitigating the shading impact significantly. Further, the performance of the existing OSB, SKP, LS, MDS, SMT, and NOS is also almost on par with the proposed ones under this shading. Following these, the puzzle-based SDK, FP, IS, ADV, CS, analytical-based OEP, and the chaotic-based CB techniques augment the GMP by about 31.5%. The existing NCI, NA, and HM techniques deliver a sub-optimal result yielding an enhancement in the range of (25.43–26.65) %. The number-based OE performs poorly once again, resulting in the lowest GMP enhancement among all the considered strategies.

During Case-5, the effectiveness of the considered configurations is validated under a typical diagonal shading as shown in Fig. 9(a). The proposed GJ, EUT, and EQT, and the existing CB, HM approaches disperse the shade discriminately thereby yielding the optimal output. In

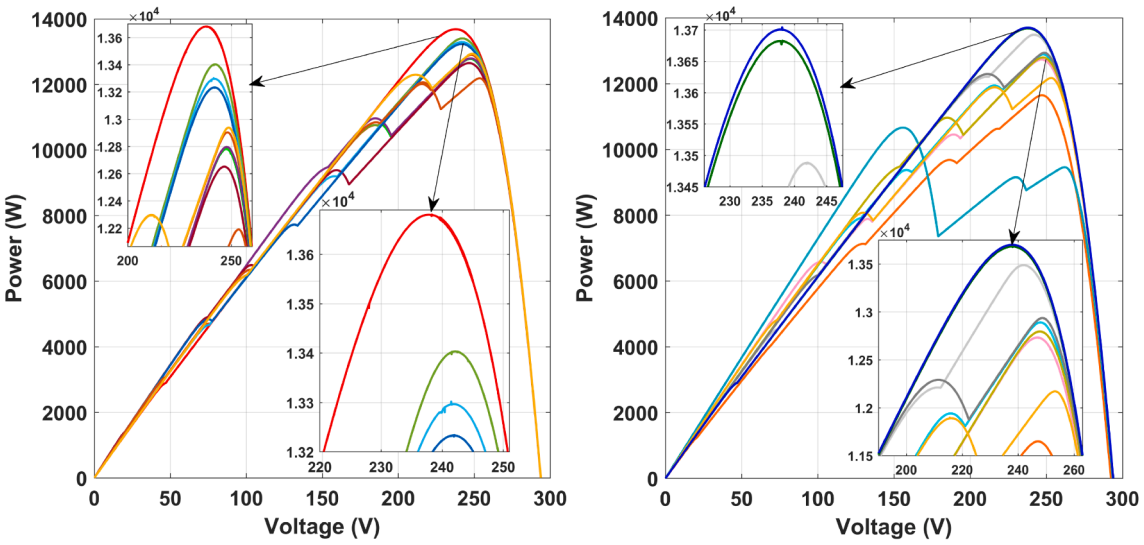

(e) Case-5

Fig. 10. (*continued*).

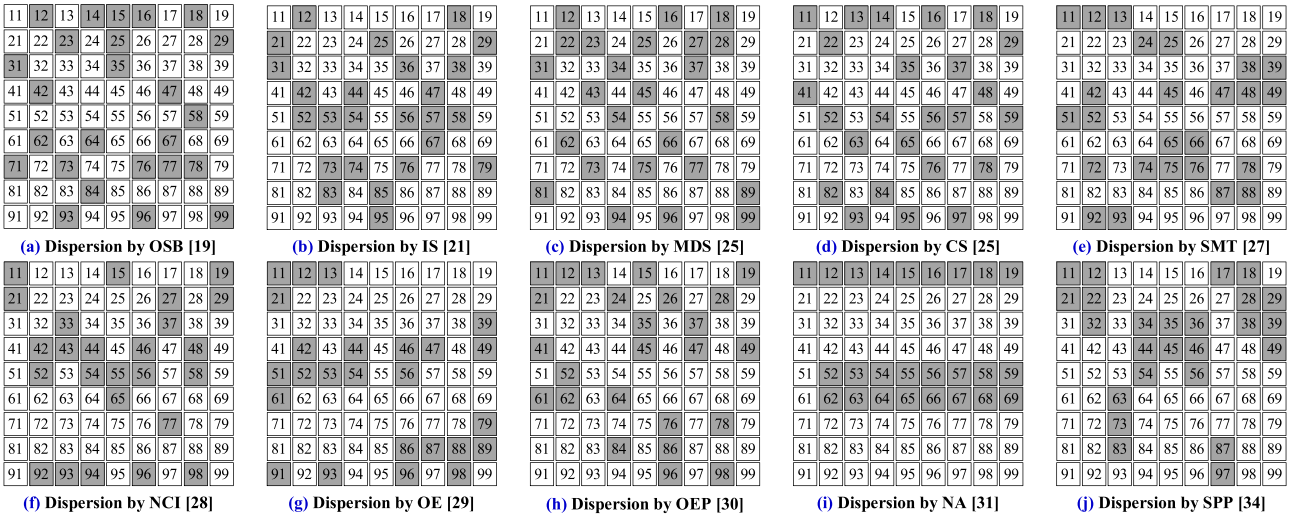

(a) Dispersion by OSB [19] (b) Dispersion by IS [21] (c) Dispersion by MDS [25] (d) Dispersion by CS [25] (e) Dispersion by SMT [27]

(f) Dispersion by NCI [28] (g) Dispersion by OE [29] (h) Dispersion by OEP [30] (i) Dispersion by NA [31] (j) Dispersion by SPP [34]

Fig. 11. Shade dispersion by various existing approaches (a)-(j) for Case-5 shading.

contrast, all other existing techniques underperform significantly (from Fig. 12) because of non-uniform shade dispersal (as shown in Fig. 11) due to their arbitrary approach of reconfiguring the array. In this case, the conventional TCT configuration yields 13704 W, whereas all the exiting techniques deliver much lower power compared to TCT. For instance, the puzzle-based SKP, OS, FP, NOS, and ADV yield 12937 W, 13234 W, 13302 W, 13403 W, 13488 W which are lowered by 5.6%, 3.43%, 2.93%, 2.20%, and 1.58% respectively. Besides, the existing SDK, OSB, SMT, NCI, IS, SKP, OE, OEP, CS, and MDS techniques deliver quite inferior performance lowering the output in the range of (5 to 10) %. Furthermore, the LS and the SPP also yield undesirable results mitigating the GMP by 14.85% and 11.04% respectively. Similarly, due to the high diagonal correlation between the panels of the array in NA configuration (as shown in Fig. 11), it delivers the most substandard performance lowering the GMP by 22.06%.

It can be noticed from Fig. 12 that certain (few) techniques exhibited performance on par with the proposed strategies in some cases, but it is clearly evident that those existing techniques have yielded inferior performance in the remaining cases. Their reliability is highly questionable due to their highly inconsistent results for all the five cases: for example, the existing IS strategy [18] yielded the GMP enhancement of utmost 9.97% (in Case-1) which is good but its performance in other respective cases are 8.41%, 1.3%, 31.39%, −11.09% which clearly shows that the IS strategy is not only highly inconsistent but also unreliable. Whereas, for the same cases (2–5), all the proposed strategies yielded GMP enhancement of 10.07%, 4.01%, 32.62%, 0%. In Fig. 13, the comparison of the proposed techniques with the OSB, IS, FP, OS are highlighted among the existing 17 techniques because these existing techniques performed slightly on par with the proposed ones in few cases and the remaining 13 techniques are considerably inferior to proposed ones in all the cases. It is noted from Figs. 9-13 that the proposed ones offered best performance under all shading cases, whereas the existing ones performed better only under few cases and inferior performance under majority cases.

Apart from the consistency of any strategy, another crucial characteristic to be considered is scalability/compatibility of a strategy. As the significance of the strategy's consistency is completely futile and becomes baseless if it cannot be scalable/compatible in the first place. For suppose the existing OSB [18] and IS [21] which are puzzle-based strategies are proven to be scalable just for few symmetrical PV arrays

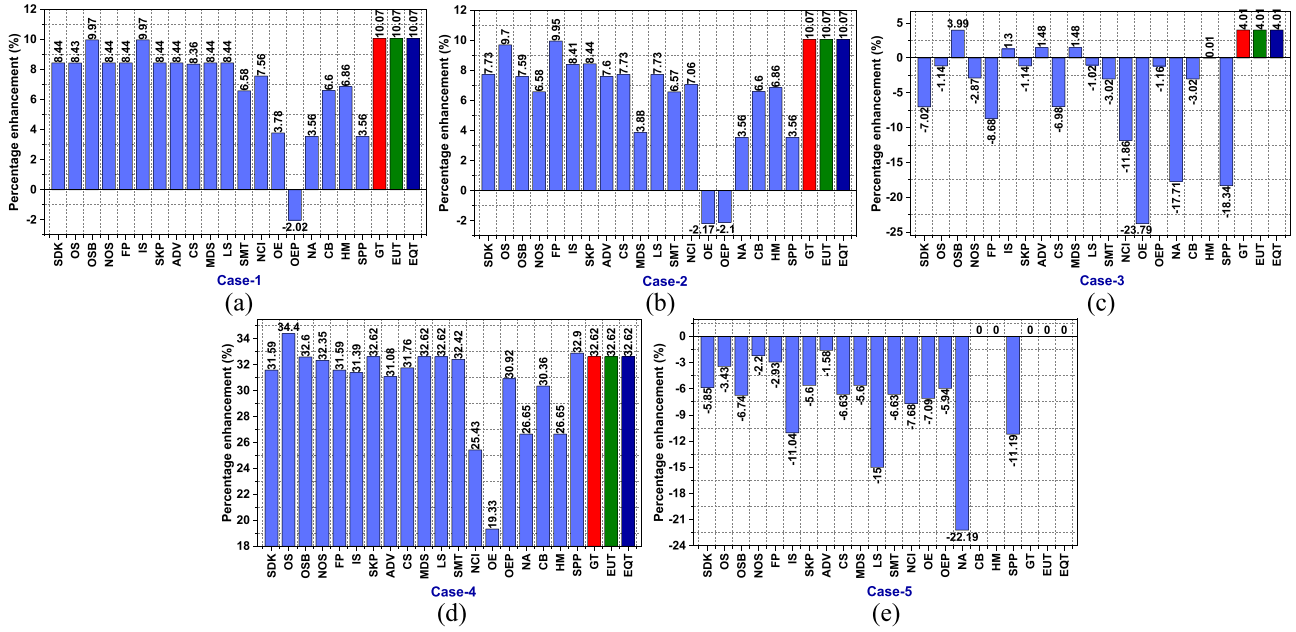

Fig. 12. GMP enhancement (in percentage) of 9 × 9 array during (a) Case-1 to (b) Case-5.

Shading case	Proposed			Existing			
	GT	EUT	EQT	OSB	IS	FP	OS
Case-1	✓	✓	✓	✓	✓	×	×
Case-2	✓	✓	✓	×	×	✓	×
Case-3	✓	✓	✓	✓	×	×	×
Case-4	✓	✓	✓	✓	–	–	✓
Case-5	✓	✓	✓	×	×	×	×

Consistent + superior results & importantly scalable to all array sizes

Inconsistent + inferior results Not scalable to all array sizes

*['✓' indicates best performance; '×' indicates inferior performance]

Fig. 13. Comparison of strategies in terms of consistency and scalability.

and are undoubtedly not scalable for the unsymmetrical arrays. So, keeping in view of the above-mentioned factors, the most pragmatic approach should be obtaining consistency and scalability hand in hand. From the in-depth analysis of the various existing strategies for 9 × 9 PV array, the proposed strategies offer a consistent, superior and performance reliability under all shading conditions. Due to the intelligent shadow dispersal strategy through optimal reconfiguration of panels by the proposed approaches, the row current mismatching between various rows has been mitigated significantly. Further, to strengthen the analysis, the proposed GT approach is tested under a few more common shadowing cases depicted in Fig. 14. The other two proposed approaches also yield the same results. It is observed from the figure that the proposed GT exhibit superior shade dispersion during all conditions with significant enhancement in the GMP.

5.2. Study on unsymmetrical 5 × 10 PV array

The feasibility and effectiveness of the proposed approaches have been validated for a medium-range 5 × 10 unsymmetrical PV array for six different shadowing cases (shown in Fig. 15). Except for a few, almost all existing static reconfiguration approaches [17–28,31–32] are compatible and scalable for unsymmetrical PV arrays. Very recently, the analytical-based Odd-even (OE), and Odd-Even-Prime (OEP) approaches have been proposed to reconfigure the unsymmetrical PV arrays to mitigate the shading impact. The effectiveness of the proposed GT, EUT, and EQT has been proven once again for the unsymmetrical arrays since they yield the highest GMP under all shading conditions (from Table.3). Further, due to the intelligence involved in the reconfiguration process reducing the correlation between neighboring modules, the shade is uniformly dispersed thereby balancing the irradiations in all rows. This remarkable and distinctive feature of the proposed approaches has led to significant enhancement in the obtained array characteristics with reduced MPPs.

The reduction in MPPs is highly advantageous for the MPPT controllers in detecting and tracking the GMP within a short span. It is remarked from Fig. 16 that the PV characteristics obtained by the proposed approaches have only one power peak facilitating the better functionality and reduced cost of MPPT controllers. On the other hand, the existing OE, OEP, and conventional TCT yield lowered output with numerous power peaks making the detection and tracking of GMP a challenging task for the MPPT controllers. Hence, it is noteworthy to state that the proposed techniques not only maximize the GMP but also enhance the array characteristics minimizing the no. of MPPs.

5.3. Experimental validation of the proposed approaches

The laboratory and the outdoor experimental prototype models of the proposed GT, EUT, and EQT reconfiguration approaches have been developed for a 4 × 4 array as depicted in Fig. 17. The prototype test bench contains sixteen 3-Watt PV panels, a solar irradiation emulator comprised of numerous double ended halogen bulbs having a control knob to regulate the intensity, a variable sliding adjustable rheostat that operates as a load, banana connector plugs to re-configure the PV array in distinct configurations, few interconnecting ties for connecting the panels, transparent polythene sheets to limit the incident irradiation to simulate different shading conditions. The specifications of the PV panels used in the experimentation has been given in Table.5 of Appendix. To measure the PV array current and voltage, two SM7023A auto-range digital multimeters were installed in series and parallel to the PV array.

Homogeneous irradiation levels are maintained across all PV panels due to the proper placement of halogen lights over the panels. The

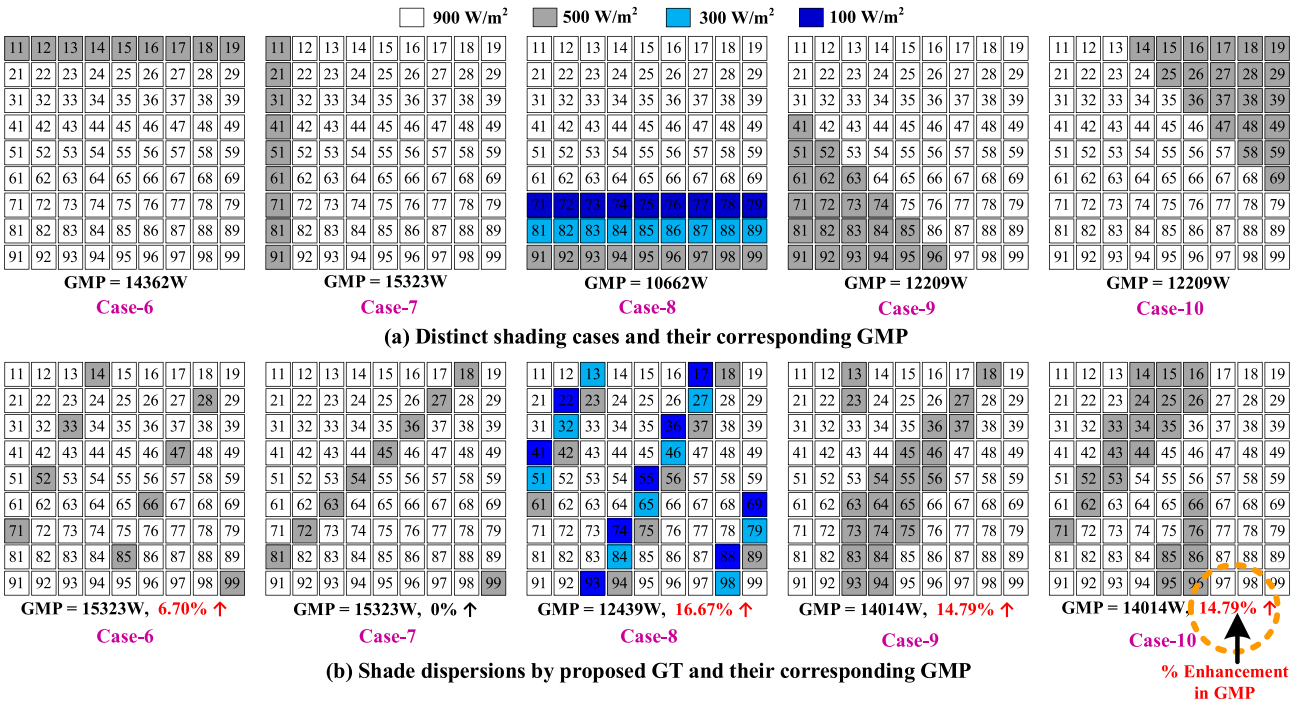

Fig. 14. (a) Additional shading cases of 9 × 9 array and (b) the corresponding dispersion by proposed GT approach.

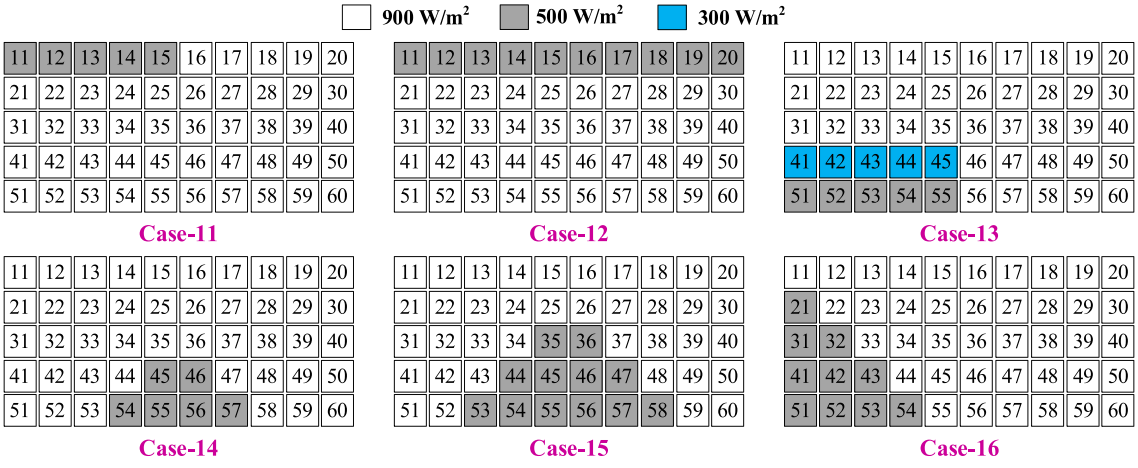

Fig. 15. Distinct shading cases of 5 × 10 array.

Table 3
Obtained GMP (in Watt) for 5 × 10 array under Case-11 to Case-16.

Approach	Case-11	Case-12	Case-13	Case-14	Case-15	Case-16
TCT [8]	8371.1	7952.0	7309.3	8756.5	7780.9	8615.8
OE [29]	8389.7	8114.2	7318.7	9307.8	8556.1	8251.0
OEP [30]	9135.1	8516.2	8198.8	8351.8	7796.4	8842.1
Proposed GT	**9515.5**	**9023.2**	**8818.8**	**9362.7**	**8762.0**	**9021.6**
Proposed EUT	**9515.6**	**9022.3**	**8818.8**	**9309.0**	**8562.9**	**9021.5**
Proposed EQT	**9516.6**	**9024.3**	**8819.8**	**9366.7**	**8763.0**	**9022.3**

irradiation from a single halogen light can generate 400 W/m^2. The incidence irradiance and operating panel temperature are measured using a TM-206 digital solar power meter and a carent HTD8813C digital infrared temperature gun. The positive and negative tapings are provided on each PV module of the prototype, allowing it to be reconfigured through banana plug connections in distinct configurations. The array terminals are interconnected to a variable rheostat, that could be adjusted to fix the resistance value for maximizing the power harvesting from array. No additional electric and electronic equipment or devices are needed for hardware execution since the proposed topologies are fixed and static. The developed 4 × 4 conventional TCT PV array yields 17.2 W under unshaded conditions in the indoor experimentation, with operational temperature and incident irradiation from the irradiation simulator measured to be about 320 W/m^2 and 29 °C respectively.

- The performance of proposed approaches for a symmetrical 4 × 4 array is tested indoors under Case-17 to Case-20 shading scenarios.
- Besides, for better practical realization, they are also tested outdoors under different shadowing conditions as illustrated in Case-21 to Case-24 of Fig. 18. The unshaded and shaded panels in the outdoor environmental setup are measured to receive about 700 W/m^2 and 250 W/m^2 irradiances.

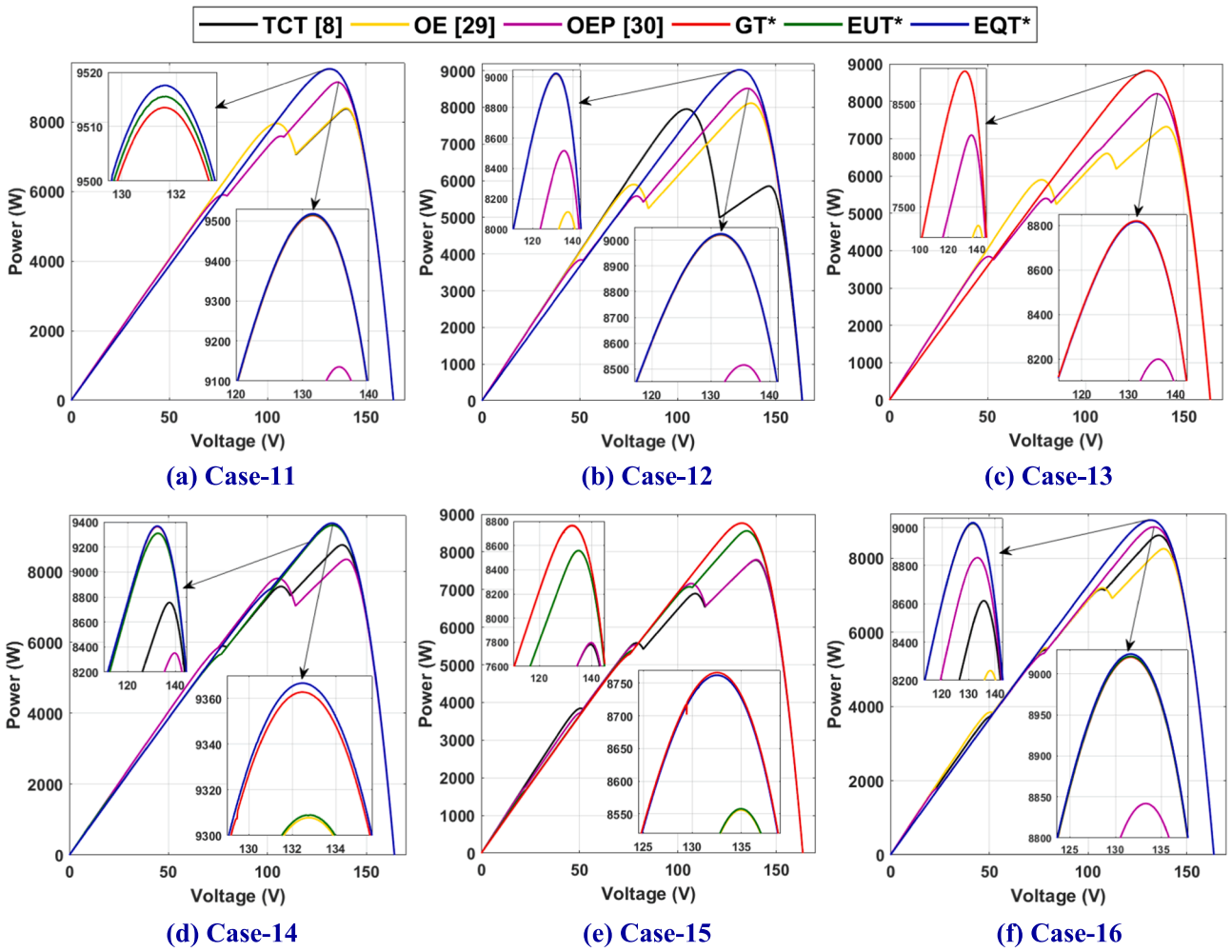

Fig. 16. Power-voltage characteristics of 5 × 10 unsymmetrical array under (a) Case-11 to (f) Case-16.

- The performance of proposed techniques is contrasted with the conventional TCT, and very recent OE [29] and OEP [30] approaches.

The obtained array's PV characteristics under these cases are shown in Fig. 20. It is noted from the figure that the highest output is obtained by the integer sequence-based proposed approaches due to their superiority in evenly dispensing the shade over array. The OE and OEP approaches, on the other hand, yield lower performance due to arbitrary process of reconfiguration, while being scalable to unsymmetrical arrays. In the evaluated eight shading-

-cases, the existing OE and OEP yields the highest output only in 2 out of 8 and 3 out of 8 cases, respectively, whereas all the three proposed GT, EUT, EQT yield highest output under all the considered 8 cases exhibiting superior and consistent performance. Further, the obtained experimental results (in Fig. 19) are compared with that of the simulation results (in Fig. 20) and both are found to be close to each other. From the qualitative and comprehensive investigation, it has been ascertained that the proposed integer sequence-based encryption approaches are highly preferred for reconfiguring both the unsymmetrical and symmetrical array sizes.

6. Qualitative comparison of proposed techniques with state-of-the-art techniques

The efficiency of the proposed approaches in comparison to the contemporary state-of-the-art methods in terms of distinct parameters has been tabulated in Table.4.

- Unlike the AI approaches [8–9] like Fuzzy logic-based, the proposed approaches does not involve switching matrix, optimum switching matrix selection and further eliminates the memory-related issues for switching matrix operation.
- The EAR-based strategies [10–11] require a controller to provide the switching pulses for power electronic switches in accordance with the required shade dispersion. Additionally, they need a lot of switching patterns to identify the optimal way to reconfigure a PV array. On contrary, the proposed strategies eliminate the need for these steps.
- The proposed techniques evade the drawbacks of population-based metaheuristic optimization algorithms [12–16] such as high dimensional search space, convergence & parameter selection-related issues, methodology issues, being stuck at local optimum, weighting factor selection challenges, massive computations, high computation time, etc.
- Contrary to the existing puzzle-based and logic-based methodologies [17–25], the proposed approaches are fully scalable and compatible with all array sizes of array. Further, the proposed configurations disperse the shade discriminately and uniformly through the intelligence involved in their encryption-based methodology process.
- The proposed reconfiguration methodologies successfully rectify numerous drawbacks of the existing magic square-based [26], shift-based [27,31], and index-based [28] approaches, including poor

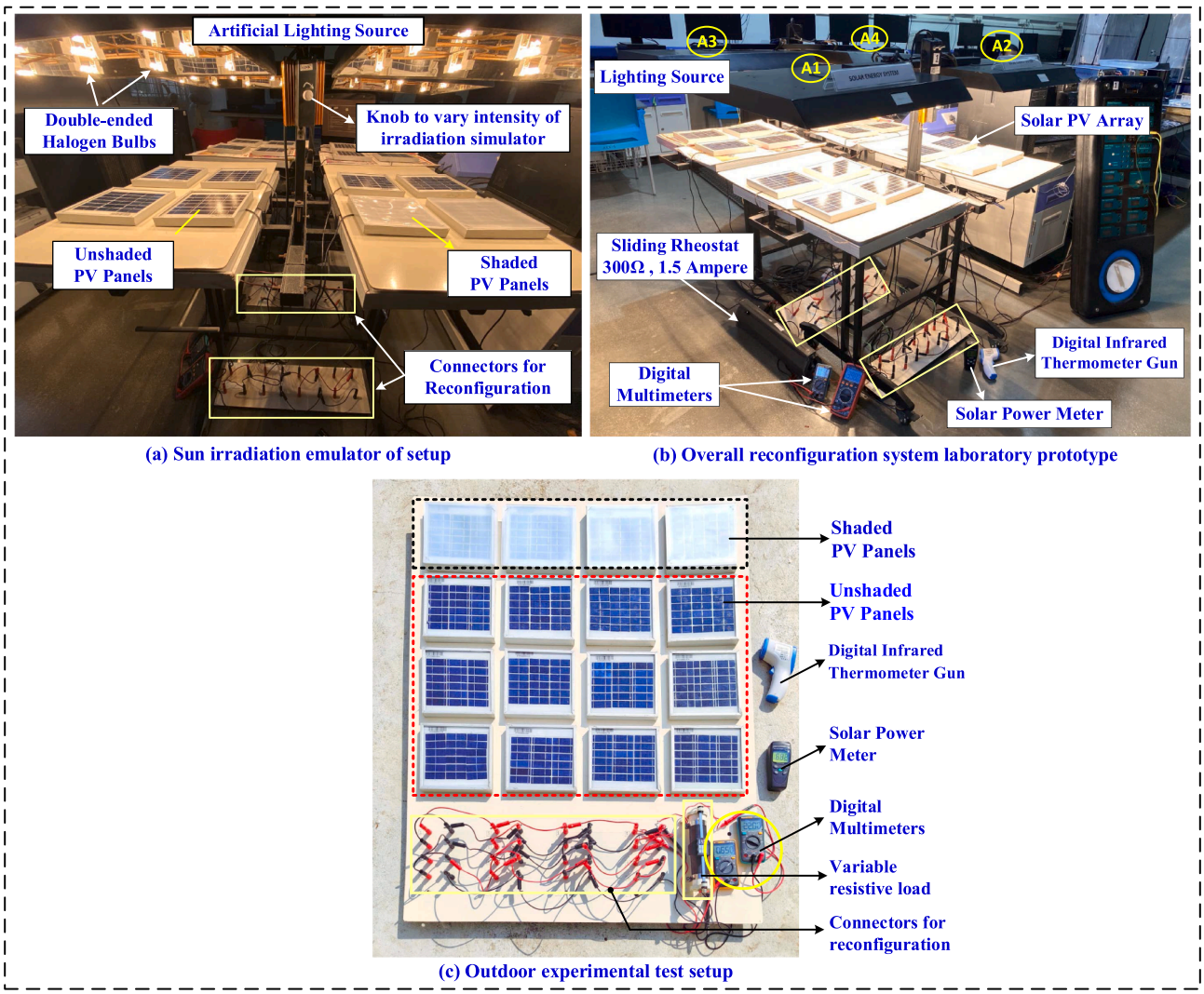

Fig. 17. Experimental prototype setup of reconfiguration system in (b) laboratory and (c) outdoors.

scalability, a high correlation between the diagonal arrangement of panels, inconsistency, etc.

- The analytic-based OE [29] and OEP [30] techniques, despite being scalable to any array size yield inconsistent performance possessing a high correlation between the adjoint shaded panels row-wise. In comparison, the proposed ones are not only universally compatible but also consistently superior under shading conditions.
- In chaotic approaches [32–33], there exists a very high correlation between the row-wise panels and the diagonally arranged panels thereby exhibiting a significant mismatch in the PV array. In contrast, the proposed approaches significantly mitigate the correlation between the adjoint shaded panels (in the column, row, and diagonal directions) reducing the row current mismatch in the array.

7. Conclusions

The extensive literature on different reconfiguration strategies is thoroughly explored, along with the benefits and drawbacks of each. Most existing strategies suffer scalability and practical feasibility issues, exhibiting arbitrary shade dispersal and distorted array characteristics. Hence, three novel PV array reconfiguration approaches have been proposed using integer sequence-based image processing to optimize the array output by mitigating the mismatch under PSC. The proposed approaches overcome the drawbacks of the existing ones.

- The proposed strategies have been extensively studied for different symmetrical 9 × 9, 4 × 4 and 5 × 10 unsymmetrical PV arrays using the power-voltage characteristics.
- The effectiveness of the proposed strategies has been analyzed and contrasted with the 20 existing strategies during diverse 24 shading conditions.
- On contrary to existing approaches, the proposed ones disseminate the shade intelligently by optimally reconfiguring the array using the encrypted matrices obtained by the integer sequence-based transforms equalizing the irradiation and mitigating the mismatch.
- An experimental hardware prototype model has been developed and tested on a 4 × 4 PV array in the laboratory and outdoor environments under eight distinct shading conditions.

It is remarked from the overall analysis that the performance of the proposed strategies is on par with each other yielding superior and consistent performance with significantly enhanced PV array characteristics and reduced peaks. This distinctive feature facilitates the easy and rapid tracking of GMP by the MPPT controllers further eliminating the need for advanced, complex, and sophisticated controllers. Therefore, employing the proposed intelligent reconfiguration approaches ensures the extraction of optimal power from the partially shaded PV arrays rapidly and confirms to be the need of the moment.

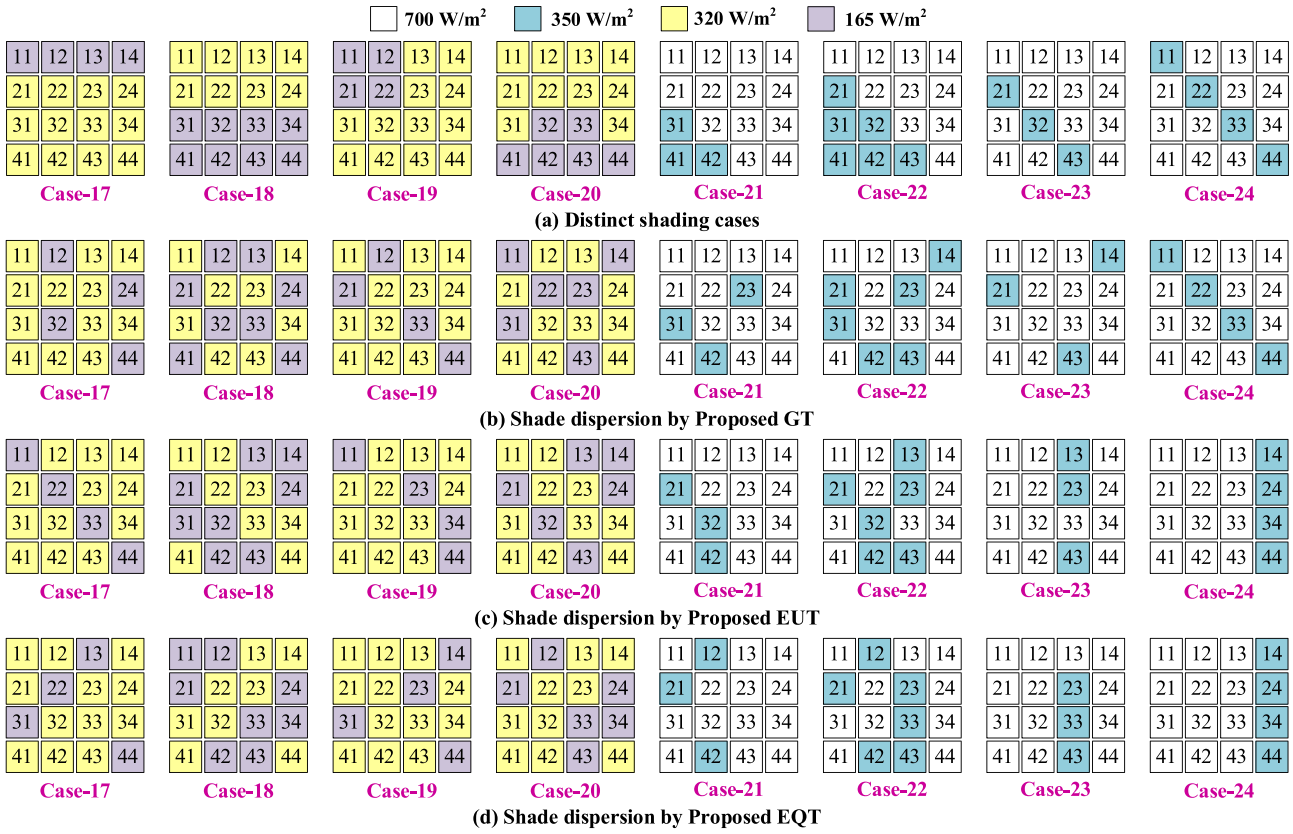

Fig. 18. (a) Different shading cases and (b)-(d) respective shade dispersal by proposed approaches of 4 × 4 array.

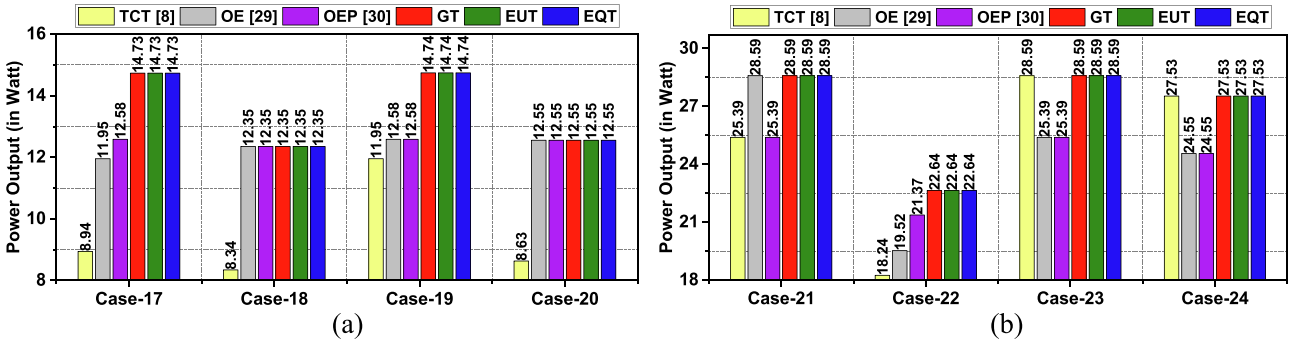

Fig. 19. Obtained experimental results in (a) indoor laboratory and (b) outdoor environment.

8. Future scope

In the future, these strategies can be adapted in dynamic array reconfiguration processes to determine the optimized switching matrix pattern. Implementing this into operation can circumvent the drawbacks of metaheuristic and distinct optimization algorithms. Additionally, integrating the MPPT control strategies to the proposed cryptographic-based reconfiguration strategies for tracking the maximum power can be further explored for residential rooftops, commercial, and utility-scale PV installations.

Data availability statement

Data sharing is not applicable to this article as no new data were created or analyzed in this study.

CRediT authorship contribution statement

Kanasottu Anil Naik: Project administration, Resources, Software, Supervision, Validation, Visualization, Writing – review & editing. **Rayappa David Amar Raj:** Conceptualization, Methodology, Formal analysis, Writing – original draft, Software, Investigation. **Chepuri Venkateswara Rao:** Conceptualization, Methodology, Formal analysis, Writing – review & editing, Investigation, Visualization. **Thanikanti Sudhakar Babu:** Formal analysis, Investigation, Resources, Writing – review & editing, Supervision.

Declaration of Competing Interest

The authors declare that they have no known competing financial interests or personal relationships that could have appeared to influence the work reported in this paper.

Data availability

No data was used for the research described in the article.

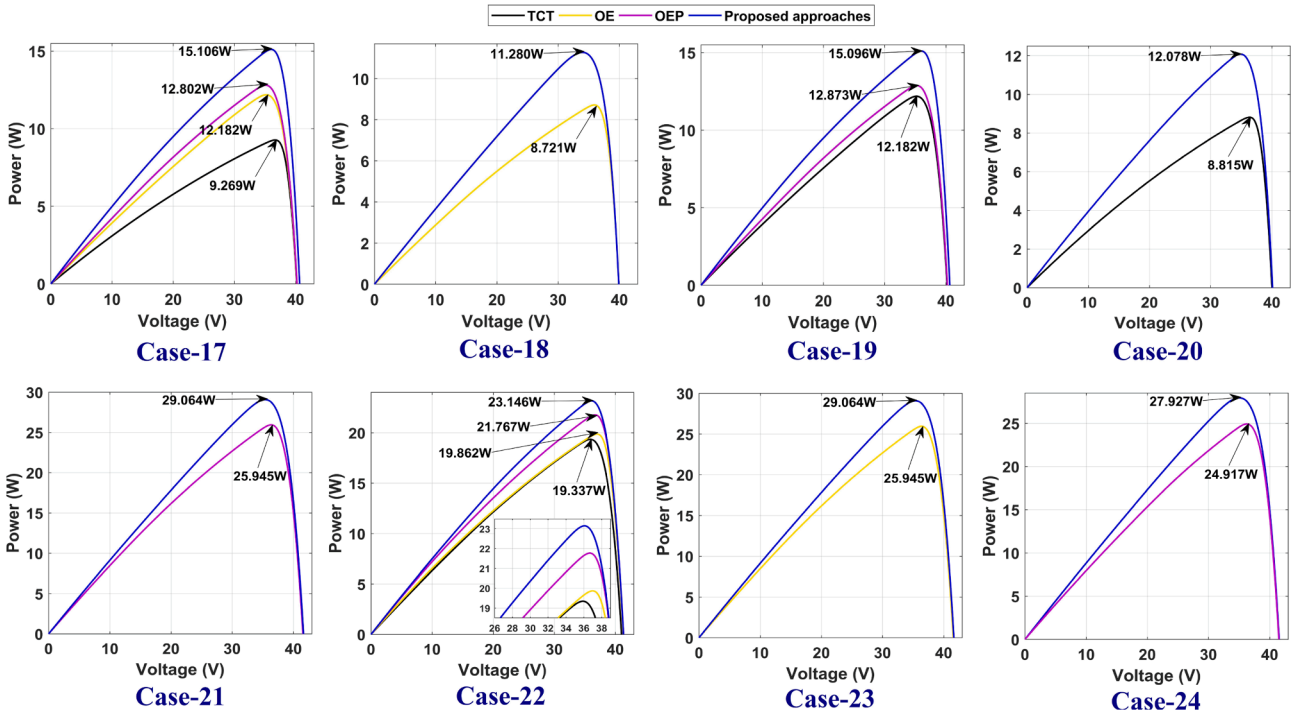

Fig. 20. PV characteristics obtained under (a) Case-17 to (h) Case-24.

Table 4
Qualitative comparison of various reconfiguration strategies with proposed ones.

Technique	P_1	P_2	P_3	P_4	P_5	P_6	P_7	P_8	P_9
Conventional [8]	VH	L	–	VH	VH	–	–	VL	L
AI-based [8–9]	H	M	VL	H	H	M	VH	H	VH
EAR-based [10–11]	M	M	VL	H	H	M	VH	H	VH
Metaheuristic [12–16]	VH	H	H	L	L	H	VH	VH	VH
Puzzle-based [17–25]	L	M	M	M	M	L	–	L	L
Magic square-based [26]	VL	M	M	M	M	L	–	L	L
Shift-based [27,31]	L	M	L	H	M	VL	–	L	L
Index-based [28]	L	M	L	M	M	VL	–	L	L
Analytic-based [29–30]	VH	M	VL	VH	VH	VL	–	M	L
Chaotic-based [32–33]	M	M	M	M	H	M	–	M	L
Proposed GT, EUT, EQT	**VH**	**VH**	**VH**	**VL**	**VL**	**VH**	–	**L**	**L**

(P_1) Scalability, (P_2) GMP Yielded, (P_3) Uniform shade dispersion, (P_4) Mismatch between rows (row currents), (P_5) No. of power peaks, (P_6) Consistency, (P_7) Need for switches & sensors, (P_8) Algorithm complexity, (P_9) Total system cost. (-): Nil, L: Low, M: Medium, H: High, V: Very.

Appendix

Table 5.

Table 5
Specifications and parameters for PV panel used in experimentation.

Specification	Symbol	Rating
Maximum power	P_{MPP}	3 W
Maximum power voltage	V_{MPP}	9.01 V
Maximum power current	I_{MPP}	0.34 A
Open circuit voltage	V_{oc}	10.8 V
Short circuit current	I_{sc}	0.38 A
Number of Cells	N_{cell}	36
Dimensions		315 × 200 mm

References

[1] Shen Y, He Z, Xu Z, Wang Y, Li C, Zhang J, et al. Modeling of photovoltaic modules under common shading conditions. Energy 2022;256:124618.
[2] Raj RDA, Naik KA. A novel scan pattern for reconfiguration of partially shaded photovoltaic arrays for maximum power extraction. Int J Wiley J Circuit Theory Appl 2022. https://doi.org/10.1002/cta.3452.
[3] Ahmed S, Mekhilef S, Mubin MB, Tey KS. Performances of the adaptive conventional maximum power point tracking algorithms for solar photovoltaic system, Sustainable Energy Technologies and Assessments, 53, Part A; 2022, 102390.
[4] Nassef M, Houssein EH, Helmy BE, Rezk H. Modified honey badger algorithm based global MPPT for triple-junction solar photovoltaic system under partial shading condition and global optimization. Energy 2022;124363.
[5] Ali M, Ramadan H, Mohamed A. Improved P&O MPPT algorithm with efficient open-circuit voltage estimation for two-stage grid-integrated PV system under realistic solar radiation. Int J Electr Power Energy Syst 2022;137:107805.
[6] Sousa SM, Gusman LS, Lopes TAS, Pereira HA, Callegari JMS. MPPT algorithm in single loop current-mode control applied to dc–dc converters with input current source characteristics. Int J Electr Power Energy Syst 2022;138:107909.
[7] Belhachat F, Larbes C. PV array reconfiguration techniques for maximum power optimization under partial shading conditions: A review. Sol Energy 2021;230: 558–82.
[8] Bouselham L, Rabhi A, Hajji B, Mellit A. Photovoltaic array reconfiguration method based on fuzzy logic and recursive least squares: An experimental validation. Energy 2021;232:121107.

[9] Solis-Cisneros HI, Sevilla-Camacho PY, Robles-Ocampo JB, Zuñiga-Reyes MA, Rodríguez-Resendíz J, Muñiz-Soria J, Hernández-Gutiérrez CA. Hernández-Gutiérrez, A dynamic reconfiguration method based on neuro-fuzzy control algorithm for partially shaded PV arrays, Sustainable Energy Technologies and Assessments, 52, Part B; 2022, 102147.

[10] Velasco-Quesada G, Guinjoan-Gispert F, Pique-Lopez R, Roman-Lumbreras M, Conesa-Roca A. Electrical PV Array Reconfiguration Strategy for Energy Extraction Improvement in Grid-Connected PV Systems. IEEE Trans Ind Electron 2009;56(11):4319–31.

[11] Raj RD, Bhattacharjee S, Biswas M. Electrical Reconfiguration Technique for Partially Shaded PV Arrays with Minimal Interconnections. In: 2020 International Conference on Power Electronics & IoT Applications in Renewable Energy and its Control, 2020, pp. 90-95, doi: https://doi.org/10.1109/PARC49193.2020.236564.

[12] Deshkar SN, Dhale SB, Mukherjee JS, Babu TS, Rajasekar N. Solar PV array reconfiguration under partial shading conditions for maximum power extraction using genetic algorithm. Renew Sustain Energy Rev 2015;43:102–10.

[13] Babu TS, Ram JP, Dragičević T, Miyatake M, Blaabjerg F, Rajasekar N. Particle Swarm Optimization Based Solar PV Array Reconfiguration of the Maximum Power Extraction Under Partial Shading Conditions. IEEE Trans on Sustain Energy 2018;9(1):74–85.

[14] Fathy A. Butterfly optimization algorithm based methodology for enhancing the shaded photovoltaic array extracted power via reconfiguration process. Energy Convers Manage 2020;220:113115.

[15] Rezk H, Fathy A, Aly M. A robust photovoltaic array reconfiguration strategy based on coyote optimization algorithm for enhancing the extracted power under partial shadow condition. Energy Rep 2021;7:109–24.

[16] Pappachan SN. Hybrid Red Deer with Moth Flame Optimization for Reconfiguration Process on Partially Shaded Photovoltaic Array, Energy Sources A: Recovery Util. Environ. Eff.; 2022.

[17] Rani BI, Ilango GS, Nagamani C. Enhanced Power Generation From PV Array Under Partial Shading Conditions by Shade Dispersion Using Su Do Ku Configuration. IEEE Trans Sustainable Energy 2013;4(3):594–601.

[18] Krishna SG, Moger T. Optimal SuDoKu Reconfiguration Technique for Total-Cross-Tied PV Array to Increase Power Output Under Non-Uniform Irradiance. IEEE Trans Energy Convers 2019;34(4):1973–84.

[19] Horoufiany M, Ghandehari R. Optimization of the Sudoku based reconfiguration technique for PV arrays power enhancement under mutual shading conditions. Sol Energy 2018;159.

[20] Sahu HS, Nayak SK, Mishra S. Maximizing the Power Generation of a Partially Shaded PV Array. IEEE J Emerging Selected Top Power Electron 2016;4(2):626–37.

[21] Krishna GS, Moger T. Improved SuDoKu reconfiguration technique for total-cross-tied PV array to enhance maximum power under partial shading conditions. Renew Sustain Energy Rev 2019;109:333–48.

[22] Nihanth MS, Ram JP, Pillai DS, Ghias AM, Garg A, Rajasekar N. Enhanced power production in PV arrays using a new skyscraper puzzle based one-time reconfiguration procedure under partial shade conditions (PSCs). Solar Energy 2019;194:209–24.

[23] Bharti G, Tatabhatla VMR, Kanumuri T. Power maximization under partial shading conditions using advanced sudoku configuration, In: Proceedings of the International Conference on Paradigms of Computing, Communication and Data Sciences, Springer, Singapore, 2021, pp. 189-205.

[24] Anjum S, Mukherjee V, Mehta G. Hyper SuDoKu-Based Solar Photovoltaic Array Reconfiguration for Maximum Power Enhancement Under Partial Shading Conditions. ASME J Energy Resour Technol 2022;144(3):031302.

[25] Anjum S, Mukherjee V, Mehta G. Advanced SuDoKu-Based Reconfiguration Strategies for Maximum Power Extraction From Partially Shaded Solar Photovoltaic Array. ASME J Sol Energy Eng December 2021;143(6):061003.

[26] Venkateswari R, Rajasekar N. Power enhancement of PV system via physical array reconfiguration based Lo Shu technique. Energy Conv and Management 2020;215:112885.

[27] Belhaouas N, Ait Cheikh M-S, Agathoklis P, Oularbi M-R, Amrouche B, Sedraoui K, et al. PV array power output maximization under partial shading using new shifted PV array arrangements. Appl Energy 2017;187:326–37.

[28] Pillai DS, Ram JP, Nihanth MSS, Rajasekar N. A simple, sensorless and fixed reconfiguration scheme for maximum power enhancement in PV systems. Energy Conv and Management 2018;172:402–17.

[29] Yadav K, Kumar B, Swaroop D. Mitigation of Mismatch Power Losses of PV Array under Partial Shading Condition using novel Odd Even Configuration. Energy Rep 2020;6:427–37.

[30] Reddy SS, Yammani C. Odd-Even-Prime pattern for PV array to increase power output under partial shading conditions. Energy 2020;213:118780.

[31] Nihanth MSS, et al. A new array reconfiguration scheme for solar PV systems under partial shading conditions. Intelligent computing techniques for smart energy systems. Springer: Singapore; 2020. p. 387–96.

[32] Tatabhatla VMR, Agarwal A, Kanumuri T. A Chaos Map Based Reconfiguration of Solar Array to Mitigate the Effects of Partial Shading. IEEE Trans on Energy Conv 2022;37(2):811–23.

[33] Raj RDA, Naik KA. A generalized henon map-based solar PV array reconfiguration technique for power augmentation and mismatch mitigation. IETE J Res 2022:1–19. https://doi.org/10.1080/03772063.2022.2055660.

[34] Cherukuri SK, et al. Power Enhancement in Partial Shaded Photovoltaic System Using Spiral Pattern Array Configuration Scheme. IEEE Access 2021;9:123103–16.

[35] Raj RDA, Naik KA. A Novel Solar Photovoltaic Array Reconfiguration Technique Using Two-Dimensional Generalized Arnold's Cat Map. J of Solar Energy Engineering 2022;144(6):061001. https://doi.org/10.1115/1.4054506.

[36] Sloane NJA. The on-line encyclopedia of integer sequences; 2013.

[37] Chaturvedi A, Slijk W. A novel approach to determine which organism best displays Gijswijt's Sequence in its genome. J Emerg Investigators Jan 2022.

[38] Weisstein, Eric W. Euler Zigzag Number, MathWorld–A Wolfram Web Resource. https://mathworld.wolfram.com/EulerZigzagNumber.html.

[39] Shin H, Zeng J. More bijections for Entringer and Arnold families. Electronic Res Archive 2021;29(2).

[40] Santos BR. Problem 2204: Equidigital Representation. J Recreational Mathematics 1995;27:58–9.

[41] Raj RD, Kanasottu AN. An image encryption concept based solar photovoltaic array reconfiguration techniques for mismatch mitigation. Energy Sources Part A 2022;44(1):951–72. https://doi.org/10.1080/15567036.2022.2052383.

[42] Mishra M, Mishra P, Adhikary MC, Kumar S. Image encryption using Fibonacci-Lucas transformation, International J. on Cryptography and Information. Security 2012;2(3):131–41.

[43] Wang X, Gao S. Image encryption algorithm based on the matrix semi-tensor product with a compound secret key produced by a Boolean network. Inf Sci 2020;539:195–214.

[44] Raj RDA, Naik KA. Optimal reconfiguration of PV array based on digital image encryption algorithm: A comprehensive simulation and experimental investigation. Energy Convers Manage 2022;261:115666. https://doi.org/10.1016/j.enconman.2022.115666.